Title: A role for the Gram-negative outer membrane in bacterial shape determination

Authors: Elayne M. Fivenson[1], Patricia D.A. Rohs[1], Andrea Vettiger[1], Marios F. Sardis[1], Grasiela Torres[1], Alison Forchoh[1], and Thomas G. Bernhardt[1,2*]

Affiliations:
[1]Department of Microbiology, Blavatnik Institute, Harvard Medical School, Boston, MA 02115.
[2]Howard Hughes Medical Institute, Boston, United States.

***To whom correspondence should be addressed**.
Thomas G. Bernhardt, Ph.D.
Harvard Medical School
Department of Microbiology
Boston, Massachusetts 02115
e-mail: thomas_bernhardt@hms.harvard.edu

Classification: Major: Biological Sciences Minor: Microbiology

Keywords: peptidoglycan, lipopolysaccharide, morphogenesis, cell envelope

Author contributions:

E.M.F., P.D.A.R. , A.V., M.F.S. and T.G.B. designed the research. E.M.F., P.D.A.R. , A.V., M.F.S.. G.T., and A.F. performed the research. E.M.F., P.D.A.R. , A.V., M.F.S.. G.T., A.F., and T.G.B., analyzed the data. E.M.F. and T.G.B. wrote the paper.

This PDF file inclues:

- Main Text
- Figures 1-6
- Supporting Text
- Figures S1 to S5
- Legend for Movie S1
- Tables S1 to S4
- SI references

Other supporting materials for this manuscript include the following:

- Movie S1

ABSTRACT

The cell envelope of Gram-negative bacteria consists of three distinct layers: the cytoplasmic membrane, a cell wall made of peptidoglycan (PG), and an asymmetric outer membrane (OM) composed of phospholipid in the inner leaflet and lipopolysaccharide (LPS) glycolipid in the outer leaflet. The PG layer has long been thought to be the major structural component of the envelope protecting cells from osmotic lysis and providing them with their characteristic shape. In recent years, the OM has also been shown to be a load-bearing layer of the cell surface that fortifies cells against internal turgor pressure. However, whether the OM also plays a role in morphogenesis has remained unclear. Here, we report that changes in LPS synthesis or modification predicted to strengthen the OM can suppress the growth and shape defects of *Escherichia coli* mutants with reduced activity in a conserved PG synthesis machine called the Rod system (elongasome) that is responsible for cell elongation and shape determination. Evidence is presented that OM fortification in the shape mutants restores the ability of MreB cytoskeletal filaments to properly orient the synthesis of new cell wall material by the Rod system. Our results are therefore consistent with a role for the OM in the propagation of rod shape during growth in addition to its well-known function as a diffusion barrier promoting the intrinsic antibiotic resistance of Gram-negative bacteria.

SIGNIFICANCE

The cell wall has traditionally been thought to be the main structural determinant of the bacterial cell envelope that resists internal turgor and determines cell shape. However, the outer membrane (OM) has recently been shown to contribute to the mechanical strength of Gram-negative bacterial envelopes. Here, we demonstrate that changes to OM composition predicted to increase its load bearing capacity rescue the growth and shape defects of *Escherichia coli* mutants defective in the major cell wall synthesis machinery that determines rod shape. Our results therefore reveal a previously unappreciated role for the OM in bacterial shape determination in addition to its well-known function as a diffusion barrier that protects Gram-negative bacteria from external insults like antibiotics.

INTRODUCTION

Gram-negative bacteria have a characteristic three-layered cell envelope comprised of an inner (cytoplasmic) membrane (IM), a relatively thin cell wall made of peptidoglycan (PG), and an outer membrane (OM). The OM bilayer is asymmetric with phospholipids in the inner leaflet and the lipopolysaccharide (LPS) glycolipid in the outer leaflet. For many years, the PG layer was thought to be the sole load-bearing component of the envelope with the OM primarily serving to protect Gram-negative cells from external insults like antibiotics (1, 2). However, it has recently become clear that in addition to providing a barrier function, the OM can also help cells resist internal turgor pressure (3). What has remained unknown is whether the OM also partners with the PG layer to define cell shape. Here, we report a genetic analysis of PG synthesis and cell shape determination that supports such a role for the OM.

The PG heteropolymer is composed of glycan chains with alternating units of N-acetylglucosamine (GlcNAc) and N-acetylmuramic acid (MurNAc) (4). A short peptide is attached to the MurNAc sugar and is used to crosslink adjacent glycans to form the cell wall matrix. Glycosyltransferases (GTases) catalyze the polymerization of glycan polymers whereas transpeptidases (TPases) perform the crosslinking reaction. There are two major classes of PG synthases: class A Penicillin Binding Proteins (aPBPs) and complexes formed between SEDS (Shape, Elongation, Division, Sporulation) proteins and class B PBPs (bPBPs) (1, 2, 5). The aPBPs have both enzymatic functions in a single polypeptide whereas in the SEDS-bPBP complexes, the SEDS protein promotes glycan polymerization and the bPBP provides the crosslinking activity (6-9).

The SEDS-bPBP complexes RodA-PBP2 (6-8, 10) and FtsW-FtsI (9) play essential roles in rod shape determination and cell division, respectively. In both cases, these synthases are part of larger multiprotein assemblies involving cytoskeletal filaments. The rod shape determining system is called the Rod system (a.k.a. the elongasome). It promotes the elongation of bacilli and maintains their

characteristic rod shape. In addition to RodA-PBP2, the system includes filaments of the actin-like MreB protein along with three membrane proteins of poorly understood function: MreC, MreD, and RodZ (11-18). The Rod system has been observed to dynamically rotate around the long axis of the cell as it deposits new PG material to promote cell elongation. PG synthesis is required for the motion and MreB filaments are thought to orient it orthogonally to the long cell axis via a rudder-like mechanism (1, 7, 19-22).

To better understand Rod system function, we previously identified non-functional variants of MreC in *Escherichia coli* and selected for suppressor mutations that overcame their shape and viability defects (10, 23). One major class of suppressors encoded hypermorphic variants of PBP2 and RodA that provided important insight into the Rod system activation mechanism and the regulation of SEDS proteins (10). Genetic, structural, and cytological evidence suggests that MreC activates the system by inducing a conformational change in PBP2, which in turn activates RodA, shifting the complex from an inactive to an active state (10). The role of MreD in the complex is not clear (23, 24). The signals that promote Rod system activation also remain unknown, but the mechanism may involve the recognition of landmarks in the PG matrix by PBP2 (25).

In this report, we study a new class of suppressors that restore the growth and shape of *mreC* hypomorphs. Instead of activating the Rod system directly, these suppressors function by increasing the production of LPS. Further analysis of the suppression mechanism revealed that Rod system mutants are impaired for LPS production. Additionally, we found that modifications to LPS predicted to stiffen the OM restore rod shape in cells defective for MreC by promoting the feedback mechanism via which MreB orients PG synthesis. Thus, our results suggest a potential connection between Rod system activity and LPS synthesis and argue for a morphogenic role for the OM.

RESULTS

Increased LPS synthesis suppresses a Rod system defect

Cells with *mreC(R292H)* or *mreC(G156D)* mutations produce stable MreC protein capable of inducing a dominant-negative growth and shape phenotype (10, 23). Therefore, the altered proteins are likely capable of joining the Rod complex but are defective in stimulating its activity. Mutants with these alleles at the native locus can be maintained as spheres on minimal medium (M9), but they fail to grow on rich medium (LB). We selected for spontaneous suppressors that restored the growth of these mutants on LB along with their rod shape. In addition to mutants encoding altered PBP2 and RodA described previously (10), the selection also identified suppressors in the *ftsH* and *lapB*(*yciM*) genes encoding regulators of LPS synthesis (**Fig. 1, SI Table 1**). FtsH is an IM metalloprotease that along with its adapter protein LapB (26, 27) degrades LpxC (UDP-3-O-acyl-N-acetylglucosamine deacetylase) (28-30), the enzyme that catalyzes the first committed step in LPS synthesis (31, 32). Proteolysis of LpxC is in turn regulated by the essential inner membrane protein YejM (PbgA, LapC), which functions to inhibit LapB activity in a manner that is sensitive to the concentration of LPS in the IM (30, 33-38). When the steady state concentration is low due to LPS synthesis being balanced with its transport to the OM, YejM blocks LpxC turnover (**Fig. 1A, top**). However, when LPS synthesis outpaces its transport, YejM is inhibited by the buildup of LPS in the inner membrane and LpxC turnover is increased to restore homeostasis (**Fig. 1A, bottom**).

Both *ftsH* suppressors encoded protease variants with substitutions in the periplasmic loop of the protein (**Fig. 1**). One was found as a suppressor of *mreC(R292H)* and the other as a suppressor of *mreC(G156D)* (**Fig. 1, SI Table 1**). A mutation in *lapB* encoding a protein with a deletion of the last eleven C-terminal amino acids was also isolated as a suppressor of *mreC(G156D)* (**Fig. 1, SI Table 1**). Although growth rate and morphology were not restored to completely match those of wild-type cells, the suppressors supported full plating efficiency of their respective *mreC* mutant on LB (**Fig. 1B**) and switched their morphology from sphere-like to elongated rods (**Fig. 1C**). Suppression was not allele

specific as the *ftsH(V41G)* mutation originally isolated as a suppressor of *mreC(G156D)* (**SI Table 1**) also suppressed the growth and shape defects of *mreC(R292H)* (**Fig. 2A-B**).

We chose to further characterize the mechanism of suppression by the *ftsH(V41G)* allele by determining its effect on the cellular concentration of LpxC (**Fig. 2C**) and LPS (**Fig. 2D**). In cells with wild-type FtsH, mutants encoding defective MreC variants had decreased levels of both LpxC (**Fig. 2C**) and LPS (**Fig. 2D**) compared to cells with MreC(WT). The *ftsH(V41G)* allele increased LpxC and LPS levels in all cells regardless of which *mreC* allele they encoded (**Fig. 2C-D**). This change resulted in elevated levels of LPS production in cells with MreC(WT) and an increase in LPS concentration to near normal in cells with the defective MreC variants (**Fig. 2C-D**). We therefore conclude that the *ftsH(V41G)* allele is hypomorphic, leading to reduced LpxC turnover and a rise in LPS levels that compensates for the apparent defect in LPS synthesis of the *mreC* mutants.

To determine whether an increase in LPS synthesis is sufficient to suppress the defective *mreC* alleles, we overexpressed *lpxC* in the mutants (**Fig. 3**). Overproduction of LpxC indeed promoted the growth of *mreC(R292H)* and *mreC(G156D)* mutants on LB and restored an elongated rod-like shape (**Fig. 3**). However, suppression was not as robust as that promoted by the *ftsH(V41G)* allele (**Fig. 2 and 3**), suggesting either that the levels of LPS upon LpxC overproduction were too high and caused mild toxicity or that changes in the turnover of FtsH substrates other than LpxC contribute to the suppressing activity of *ftsH(V41G).* Suppression was dependent on LpxC activity as the overproduction of a catalytically defective LpxC that lacks a degradation signal (designated as ΔC5) (29, 39, 40) failed to promote the elongated growth of cells producing the MreC variants (**Fig. 3**). Notably, overexpression of *lpxC* did not suppress an *mreC* deletion (**Fig. 3**), arguing that partial Rod system activity in the *mreC(R292H)* and *mreC(G156D)* mutants is required to promote rod shape under suppressing conditions. Overall, our results suggest that the growth and shape defects of the *mreC(R292H)* and *mreC(G156D)* mutants is not just due to problems with PG biogenesis. Surprisingly, improper LPS synthesis and OM biogenesis also appear to be contributing factors.

175

176 ***mreC mutants remain capable of sensing perturbations to LPS synthesis***

177 One explanation for the decrease in LPS production observed in the *mreC* mutants is that these cells are
178 defective in modulating LpxC stability through the YejM/LapB/FtsH pathway in response to reduced LPS
179 levels (30, 33-38). To test this possibility, we monitored LpxC levels following the overproduction of a
180 hyperactive allele of *fabZ (*3-hydroxy-acyl-[acyl-carrier-protein] dehydratase) (29)*,* an enzyme that
181 functions early in the phospholipid synthesis pathway (41). Overproduction of this enzyme is expected to
182 increase the flux of common precursors into the phospholipid synthesis pathway at the expense of LPS
183 synthesis. Cells harboring the hyperactive *fabZ(L85P)* allele were previously reported to have increased
184 levels of LpxC, presumably due to LpxC stabilization in order to restore balance between the two lipid
185 biosynthesis pathways (29, 42). We found that *mreC(R292H)* cells overexpressing *fabZ(L85P)* had
186 increased levels of LpxC compared to the uninduced controls, and that the magnitude of the increase
187 was comparable to that in WT cells upon induction of the hyperactive *fabZ* allele **(Fig. 3C)**. We observed
188 a similar result when we treated *mreC(R292H)* cells with the LpxC inhibitor CHIR-090 (43, 44), which
189 was also previously shown to promote LpxC stabilization (45) (**SI Fig. 1**). Thus, *mreC* mutant cells
190 remain capable of sensing an acute reduction in LPS synthesis but fail to respond to and correct their
191 chronic deficit in LpxC and LPS levels.

192

193 ***OM modifications associated with increased stiffness suppress cell shape defects***

194 We reasoned that increasing LPS synthesis could suppress the shape defect of *mreC* mutants either by
195 activating the Rod complex similar to previously characterized suppressors in *rodA* and *mrdA* encoding
196 RodA-PBP2 (10) or by altering the structural properties of the OM. To test the former possibility, we
197 measured the effect of the *ftsH(V41G)* allele on Rod complex activity *in vivo* using a radiolabeling assay.
198 For this assay, a genetic background is used where PG synthesis by the divisome and the aPBPs can be
199 inhibited by SulA production (46-48) and (2-sulfonatoethyl) methanethiosulfonate (MTSES) treatment
200 (49), respectively. Rod system activity can be further isolated by treatment with the PBP2 specific
201 inhibitor mecillinam. This drug blocks the crosslinking activity of PBP2, but the glycosyltransferase

activity of RodA remains active, leading to an accumulation of uncrosslinked glycan chains. These uncrosslinked glycans are known to be rapidly degraded by the lytic transglycosylase Slt (49). Thus, the accumulation of nascent PG turnover products during radiolabeling in the presence of mecillinam, MTSES, and SulA can be used as an indirect measure of Rod system activity. Unlike the suppressing RodA and PBP2 variants characterized previously (10) that activate nascent PG turnover product accumulation, the *ftsH(V41G)* allele did not significantly alter Rod complex activity as assessed using the turnover assay **(SI Fig. 2**). Furthermore, the activated PBP2(L61R) variant was found to increase the resistance of cells to the MreB inhibitor A22, another indication of its ability to activate the Rod system. By contrast, overexpression of *lpxC* did not increase resistance to A22 (**SI Fig. 3**). Taken together, these results suggest that hyperactivation of LPS synthesis does not suppress the shape and growth defects of *mreC* mutants by enhancing the PG synthesis activity of the Rod complex.

To investigate whether the mechanical stabilization of the OM is the underlying mechanism by which increased LPS synthesis restores shape to the *mreC* mutants, we sought alternative ways to increase OM stiffness. LPS is composed of three covalently attached units (50). The base glycolipid is called Lipid A. It is modified by a core oligosaccharide that is conserved among Gram-negative organisms. The core is further modified by longer polysaccharide chains called O-antigens, the composition of which varies between species. Laboratory strains of *E. coli* K-12 do not synthesize O-antigen due to an insertion element in *wbbL* (51). However, it was previously reported that restoring O-antigen to the OM dramatically increases its stiffness (3). We therefore asked if re-introducing wild-type *wbbL* to the *mreC* mutants on an arabinose-inducible plasmid could suppress their growth and shape phenotypes like the overexpression of *lpxC* (**Fig. 4A**). Expression of *wbbL* but not a *lacZ* control promoted growth of the *mreC* hypomorphs under the nonpermissive condition (LB, 37˚C) and restored their growth as elongated rods (**Fig. 4B-C)**. As we observed with cells overexpressing *lpxC*, overexpressing *wbbL* did not improve the shape or growth defects of Δ*mreC* cells even though they synthesized comparable levels of O-antigen-LPS as the other strains (**Fig. 4D**). Restoring O-antigen synthesis also did not restore shape to cells deleted for *rodZ* (**SI Fig. 4**). Therefore, an intact Rod

complex is required to mediate the growth and shape changes in mutant cells with a restored O-antigen. We also investigated if other modifications to the OM can suppress rod system defects (52). We observed the overexpression of *arnT*, which catalyzes the 4-amino-4-deoxyl-L-aminoarabinose (L-Ara4N) modification of lipid A(53, 54), confers a modest but consistent improvement in growth of *mreC(R292H)* mutants under the nonpermissive condition (**SI Fig. 5A**). From these results, we infer that OM stiffening is the likely mechanism by which changes in LPS synthesis or modification restores rod shape to cells with a poorly functioning Rod system.

OM stiffness and the directional motion of MreB filaments

MreB polymers align along the greatest principal curvature of the cell and are thought to orient the insertion of new PG by the Rod system perpendicular to the long cell axis via a rudder-like mechanism (55). MreB polymers thus promote growth in a rod shape, but they also require rod shape for their proper alignment. Rod-shape is therefore thought to be a self-reinforcing property (21). We reasoned that this rod-shape feedback loop is impaired in the *mreC* mutants because the reduced activity of the Rod system fails to build an envelope robust enough to maintain the beginnings of a cylindrical extrusion that can be elongated into a rod via oriented MreB motion. However, strengthening of the OM in the suppressors may overcome this problem by stabilizing the envelope, allowing a partially functional machine to promote the self-enhancing shape determination process. To test this hypothesis, we wanted to track the motion of a functional MreB-mNeon sandwich fusion (^{SW}MreB-mNeon) (7) in *mreC* hypomorphic cells with and without shape-restoring suppressor mutations. Unfortunately, we were unable to construct strains encoding both the *mreC* hypomorphic alleles and the *^{SW}mreB-mNeon* fusion at the native locus because the combination was toxic. Instead, we produced ^{SW}MreB-mNeon from the native *mreB* locus that also contained *mreC(WT)* and overexpressed the dominant-negative *mreC(R292H)* allele from a plasmid in cells with or without O-antigen **(Fig. 5A)**. Overexpression of *mreC(R292H)* caused cells lacking O-antigen to form sphere-like cells, but the shape change was not as dramatic as that observed for cells harboring *mreC(R292H)* as the sole copy of the gene at the native locus. As expected, rod shape was maintained in O-antigen positive cells overexpressing *mreC(R292H).*

In addition to the differences in shape, the presence of O-antigen also impacted MreB dynamics. Compared to the rod-shaped O-antigen positive cells, cells lacking O-antigen showed a reduction in number of directionally moving particles and those particles that were moving did not appear to have as consistent of an orientation (**Fig. 5A, B, E, supporting movie 1**). Particles in the O-antigen positive cells were also less likely to change direction during imaging than those in the cells lacking O-antigen (**Fig. 5C**). These results argue that the OM contributes to shape determination by providing sufficient envelope stability for MreB directed PG synthesis to be properly oriented and self-reinforcing.

DISCUSSION

The OM and PG layers of the Gram-negative envelope share numerous connections. Their building blocks are synthesized from common precursors (56-58), and the layers are physically linked by PG binding proteins anchored in the OM (59-61). Additionally, the insertion of beta-barrel proteins in the OM appears to be spatially coordinated with the insertion of new PG material into the mature cell wall matrix (62). Despite these connections, it has only recently been appreciated that the OM plays a role in the mechanical stability of the Gram-negative envelope that rivals that of the cell wall (3, 63). Here, we provide evidence that rather than just stiffening the envelope, the OM also plays a critical role in rod shape determination. Additionally, our genetic analysis uncovered an unexpected connection between LPS synthesis and the activity of the Rod system that elongates the PG matrix, revealing yet another link between the two outermost layers of Gram-negative cells.

A morphogenic role for the OM is inferred from the ability of elevated LPS synthesis or O-antigen modification to restore rod-like shape to cells with a partially defective Rod system. The shape mutants showed a reduced level of LPS and the LPS synthesis enzyme LpxC **(Fig. 2)**. The stiffness of the OM is thought to be mediated by the lateral packing of LPS molecules bridged by Mg^{2+} ions (3). Thus, the OM of the shape defective cells with reduced LPS likely has suboptimal LPS packing and reduced stiffness. Increasing LPS synthesis in these cells by stabilizing LpxC or overproducing it is expected to increase

the LPS concentration in the OM of these cells, enhancing lateral interactions between LPS molecules to at least partially restore OM mechanical stability. Similarly, the addition of O-antigen is likely to stiffen the membrane despite suboptimal LPS levels because the extended glycan chains facilitate long distance LPS-LPS interactions.

How does OM stiffening rescue the Rod system defect? We propose that is does so by promoting the oriented-synthesis feedback via which the Rod system generates rod shape (21)(**Fig. 6**). A critical feature of this model of shape determination is that rod shape is self-reinforcing due to the curvature preference of MreB filaments that orients them perpendicular to the long cell axis to guide PG synthesis by the Rod system (55). If the cell wall made by the machinery is not stiff enough to hold the beginnings of a cylindrical shape in the face of turgor pressure, as is likely the case in the *mreC* mutants, then the feedback loop that elongates the cylinder to generate rod-shape cannot be initiated (**Fig. 6**). This problem is encountered in Gram-positive bacteria with defects in wall teichoic acid (WTA) synthesis (55). Much like LPS, these anionic cell wall polymers have been proposed to stiffen the envelope through lateral interactions mediated by bridging Mg^{2+} ions (21). Accordingly, mutants with reduced levels of WTA synthesis can be converted from rods to spheres by removing Mg^{2+} from the medium (55). Moreover, cell shape can be restored to *B. subtills* mutants with a partially defective Rod system by the addition of excess Mg^{2+}, which presumably rigidifies the envelope via the WTAs (64, 65). We therefore propose that the LPS of Gram-negative bacteria and WTAs of Gram-positive organisms may function similarly to promote cell shape by providing sufficient envelope rigidity to enable the self-reinforcing orientation of PG synthesis by the Rod system.

Given its relevance to antibiotic resistance, the most well-studied role of the OM is as a permeability barrier preventing the entry of bulky and/or hydrophobic drugs. Mutants defective for the Rod system have been known to have a defective OM permeability barrier for many years (11, 66), but the cause of their increased permeability to antibiotics has been unclear. Our results indicate that the problem is likely caused by a reduction in LPS synthesis in the spherical cells. Whether this reflects a direct or indirect

connection between Rod system activity and the LPS synthesis and/or transport systems is unclear. However, the *mreC* mutants we studied are still capable of responding to reductions in the flux through the LPS synthesis pathway by stabilizing LpxC **(Fig. 3C, SI Fig 1)**. Thus, the defect does not appear to be at the level of the YejM-LapB-FtsH system that monitors the steady-state level of LPS in the outer leaflet of the IM (30, 33-38). Further investigation of the LPS synthesis defect in cells with reduced Rod system activity may therefore reveal new connections between the biogenesis of the PG and OM layers of the envelope and uncover new ways to compromise the permeability barrier of Gram-negative bacteria to sensitize them to antibiotics.

METHODS

Bacterial strains and growth conditions

The strains generated and used in this study are derivatives of MG1655 and cultured in LB (1% tryptone, 0.5% yeast extract, 0.5% NaCl) or minimal (M9) medium (67). Minimal medium was supplemented with 0.2% Casamino Acids and 0.2% glucose (glu) or arabinose (ara) where indicated (see figure legends). Rod system mutants and controls were maintained on M9 + CAA + glu at 30˚C unless otherwise indicated. Strains harboring plasmids were grown in the presence of antibiotics at the following concentrations (unless indicated differently in the figure legends): 25 µg/ml chloramphenicol (CM), 25 µg/ml kanamycin (Kan), and 10 µ/ml tetracycline (Tet). All strains, plasmids, and primers used in this study are listed in **SI Tables 2, 3**, and **4**, respectively. For details, please see supplementary text.

Suppressor analysis

Suppressors were isolated and analyzed as described previously (10).

Western blots

Cells were pelleted via centrifugation and resuspended in resuspended in water and 2x Laemmli sample buffer (100 mM Tris-HCl, pH 6.8; 2% SDS; 0.1% bromophenol blue; 20% glycerol) at a 1:1 ratio to a final OD_{600} of 20, boiled for 10 minutes, and stored at -80˚C. Samples were thawed and sonicated

for 1 min twice using a Qsonica tip sonicator with an amplification of 25%. Sample concentration was determined using the Noninterfering (NI) Protein Assay (with bovine serum albumin [BSA] protein standard) (G Biosciences catalog no. 786-005). Samples were run on a 15% polyacrylamide gel (LpxC western blots) or 4–20% Mini-PROTEAN gels (BioRad cat# 4568095) and transferred to a polyvinylidene difluoride (PVDF) membrane. The membrane was rinsed in phosphate-buffered saline containing 0.1% Tween (PBS-T) (10% 10x PBS-T buffer, pH 7.4 [Sigma-Aldrich]) and blocked in 5% milk in PBS-T for 1.5 hours. The membrane was incubated in 1% milk-PBS-T containing rabbit anti-LpxC antibody (a generous gift from the Doerrler lab) or mouse anti-RpoA (anti- *E.coli* RNA polymerase alpha from Biolegend, cat# 663104) diluted 1:10,000. The membranes were incubated at 4˚C O/N rocking and then washed 4x with PBS-T at room temperature (1x quickly followed by 3x for 10 min). For LpxC blots, the membrane was incubated in 0.2% milk dissolved in PBS-T with [HRP]-conjugated anti-rabbit IgG (1:40,000 dilution, Rockland cat# 18–8816-33). For RpoA western blots, membranes were incubated with anti-mouse IgG HRP at a dilution of 1:3000 (Thermo Fisher Scientific catalog no. 34577). Membranes were incubated with secondary antibody for two hours and then washed 5x with PBS-T (1x quickly followed by 4x for 10 min per wash). Membranes were developed using the SuperSignal West Pico Plus chemiluminescent substrate (Thermo Fisher Scientific catalog no. 34577) and imaged using the c600 Azure Biosystems platform.

Detecting LPS using silver stain

Cultures were prepared as described in figure legends. For **Fig. 2**, strains listed in the figure legend were cultured for 24 hours at 30˚C in M9 + CAA + glu. Cultures were then diluted to OD_{600} = 0.05 and grown at 30˚C until OD = 0.2-0.3. Cells were gently pelleted and resuspended in LB (OD_{600} = 0.025) and grown at 37˚C until OD_{600} = 0.2-0.3. Cells were pelleted and resuspended in 1x LDS sample buffer (Invitrogen NP0008) + 4% -mercaptoethanol) to a final OD_{600} of 20. Pellets were boiled for 10 minutes and stored at -80˚C. The protein concentration of the samples was measured using the Noninterfering (NI) Protein Assay (with bovine serum albumin [BSA] protein standard) (G Biosciences catalog no. 786-005). RpoA western blots were carried out as described above. For the LPS silver stain, 50 µL of sample was

incubated with 1.25 µL of proteinase K (NEB P8107S) for 1 hour at 55˚C then 95˚C for 10 min. 20 µg (volume equivalent) was resolved on a 4-12% Criterion XT Bis-Tris gel (Bio-Rad 3450124) at 100V for 2 hours. LPS detection via silver stain was performed as described previously (68). First, the gel was fixed overnight in a solution of 200 mL of 40% ethanol and 5% acetic acid. Periodic acid was added to the fixative solution (final concentration of 0.7%). Following a 5 min incubation at room temperature, the gel was washed with 200 mL ultrapure H_20 (2x for 30 min, 1x for 1 hour). The gel was then incubated with 150 mL of staining solution (0.018 N NaOH, 0.4% NH_4OH, and 0.667% Silver Nitrate) for 10 min. The gel was then washed 3x for 15 min in 200 mL ultrapure H_20 and developed in developer solution (0.26 mM Citric Acid pH 3.0, 0.014% formaldehyde). The reaction was stopped by removing the developer and replacing it with 100 mL of 0.5% acetic acid. The gel was imaged using the Bio-Rad ChemiDocTM MP Imaging System.

Detecting LPS using Pro-Q Emerald 300 lipopolysaccharide gel stain kit

WT (HC555), *mreC(R292H)* (PR5), *mreC(G156D)* (PR30), and Δ*mreC* (EMF150) expressing *wbbL* or *lacZ* from an arabinose-inducible promoter were incubated for 24 hours in M9 + CAA + glu + tet at 30˚C and diluted to OD_{600} = 0.05 in M9 +CAA + ara + tet for 3 hours at 30˚C. After 3 hours, the cultures were gently pelleted and resuspended in LB + ara + tet. Cells were grown for an additional 2 hrs at 37˚C. Cells were pelleted and resuspended in 1x LDS sample buffer (Invitrogen NP0008) + 4% 2-mercaptoethanol) to a final OD_{600} of 20, boiled for 10 minutes, and stored at -80˚C. The protein concentration of the samples was measured using the Noninterfering (NI) Protein Assay (with bovine serum albumin [BSA] protein standard) (G Biosciences catalog no. 786-005). RpoA western blots were carried out as described above. For the LPS proemeraldQ stain, 50 µL of sample was incubated with 1.25 µL of proteinase K (NEB P8107S) for 1 hr at 55˚C then 95˚C for 10 min. A normalized volume equivalent to 20 µg total protein in the predigested sample was resolved on a 4-12% Criterion XT Bis-Tris gel (Bio-Rad 3450124) at 100V for 2 hours. The Proemerald Q stain was performed following the manufacturer's instructions (Pro-Q Emerald 300 lipopolysaccharide gel stain kit-Molecular Probes P20495). The gel was imaged using the Bio-Rad ChemiDocTM MP Imaging System.

Phase contrast microscopy

Phase contrast micrographs in **Fig. 1, 2, 3, 4, SI 4**, and **SI 5** were all taken using cells fixed in 2.6% in formaldehyde and 0.04% glutaraldehyde. After adding the fixative, cells were incubated at room temperature for 1 hour and stored at 4°C for a maximum of three days. To image, cells were immobilized on agarose pads (2%) on 1 mm glass slides (1.5 coverslips). Micrographs in **Fig. 1** were taken using a Nikon TE2000 inverted microscope using a 1.4 NA Plan Apo Ph3 objective and Nikon Elements Acquisition Software AR 3.2. Micrographs in **Fig. 2** were taken with a Nikon Ti Inverted Microscope using a 1.4 NA Plan Apo 100x Ph3 DM objective and with Nikon Elements 4.30 Acquisition Software. Micrographs in **Fig. 3, 4, SI 3**, and **SI 4** were taken with a Nikon Ti2-E inverted microscope using a 1.45 NA Plan Apo 100x Ph3 DM objective lens and Nikon Elements 5.2 Acquisition Software. Micrographs were processed using rolling ball transformation (radius = 35 pixels) in FIJI (69) prior to length and width quantification using the microbeJ plugin (70). Aspect ratio was calculated by dividing the length measurements by the width measurements. The data was plotted in Graphpad Prism and statistical analysis of aspect ratio done in GraphPad Prism using a parametric unpaired T test assuming gaussian distribution but not equal standard deviation (Welch's correction). Images were cropped in FIJI (69).

***3H-mDAP physiological radiolabeling*:** Peptidoglycan turnover was determined as described previously (7, 10, 49). Data was plotted on GraphPad Prism.

MreB Dynamics

wbbL(INS) (AV007) or *wbbL*+ (EMF210) cells expressing *mreC(R292H)D* (pMS9) were back diluted from overnight cultures (1:200) and grown in LB + 1 mM IPTG and incubated at 37˚C until OD_{600} = ~0.4. Cells were then back diluted a second time to OD_{600} = 0.05 in LB + 1 mM IPTG and incubated at 37˚C until OD_{600} = ~0.4. # 1.5 high precision coverslips (Marienfeld) were added to a hydrochloric acid and ethanol and cleaned. Cells were placed onto a 2% (w/v) agarose pad in LB + 1 mM IPTG and imaged at RT on a Nikon Ti inverted microscope equipped with Nikon TIRF Lun-f laser illumination, a Plan Apo 100x, 1.45

NA Ph3 objective lens. Images were recorded using an Andor Zyla 4.2 Plus sCMOS camera and Nikon Elements 4.30 acquisition software. Three-minute timelapse series with an acquisition frame rate of 3s were recorded to capture MreB dynamics and overlayed over a single-frame phase contrast reference image using Fiji (69). Particle tracking was performed as described in Navarro et al. (71). Briefly, MreB tracks were detected in TrackMate v6.0.1(72) using LoG detector (0.3 µm radius) and Kalman filter. To analyze the nature of the displacement of each track, the mean square displacement (MSD) was calculated using the MATLAB class msdanalyzer (73). Slopes (α) of the individual MSD curves were extracted using the Log-log fit of the MSD and the delay time τ. As the maximum delay time 75% of the track length was used. Only tracks which persisted for longer than 4 timepoints (12s) and with a R^2 for $\log[MSD]$ versus $\log[t]$ above 0.95 were included in the analysis. MreB filaments engaged in active cell wall synthesis are displaced by the action of the enzymatic activities of RodA and PBP2b (2, 7, 17-20, 22, 74) and thus it's MSD curves display slopes of $\alpha \approx 2$ indicative of a transported particle motion above the rate of Brownian diffusion ($\alpha \approx 1$) or confined motion ($\alpha > 1$). Mean directional change rate was derived from TrackMate and is defined as a measure of the angle between two succeeding links, averaged over all the links of a track and is reported in radians.

ACKNOWLEDGEMENTS

We would like to acknowledge all the members of the Bernhardt and Rudner labs for their advice and thoughtful comments throughout the course of this work. We also thank Paula Montero Llopis and the other members of the MicRoN (Microscopy Resources on the North Quad) team at Harvard Medical School for their expertise, support, consultation, and services. We thank Bill Doerrler for the generous gift of the anti-LpxC antibody. We thank Andrew Darwin (NYU) and Teru Ogura (Kumamoto University, Japan) for sharing with us the *fabZ(L85P)* mutant and Natividad Ruiz for sharing the *wbbL*+ strain NR2528. This work was supported by the National Institutes of Health (R01 AI083365 and U19 AI158028 to T.G.B.) and Investigator funds from the Howard Hughes Medical Institute (T.G.B.). E.M.F. is supported by the National Science Foundation (NSF) Graduate Research Fellowship award. P.D.A.R. was supported in part by a predoctoral fellowship from the Canadian Institute for Health Research. A.V.

is supported by a EMBO long-term postdoctoral fellowship (ALTF_89-2019) and a SNF Postdoc Mobility fellowship (P500PB_203143).

FIGURES 1-6

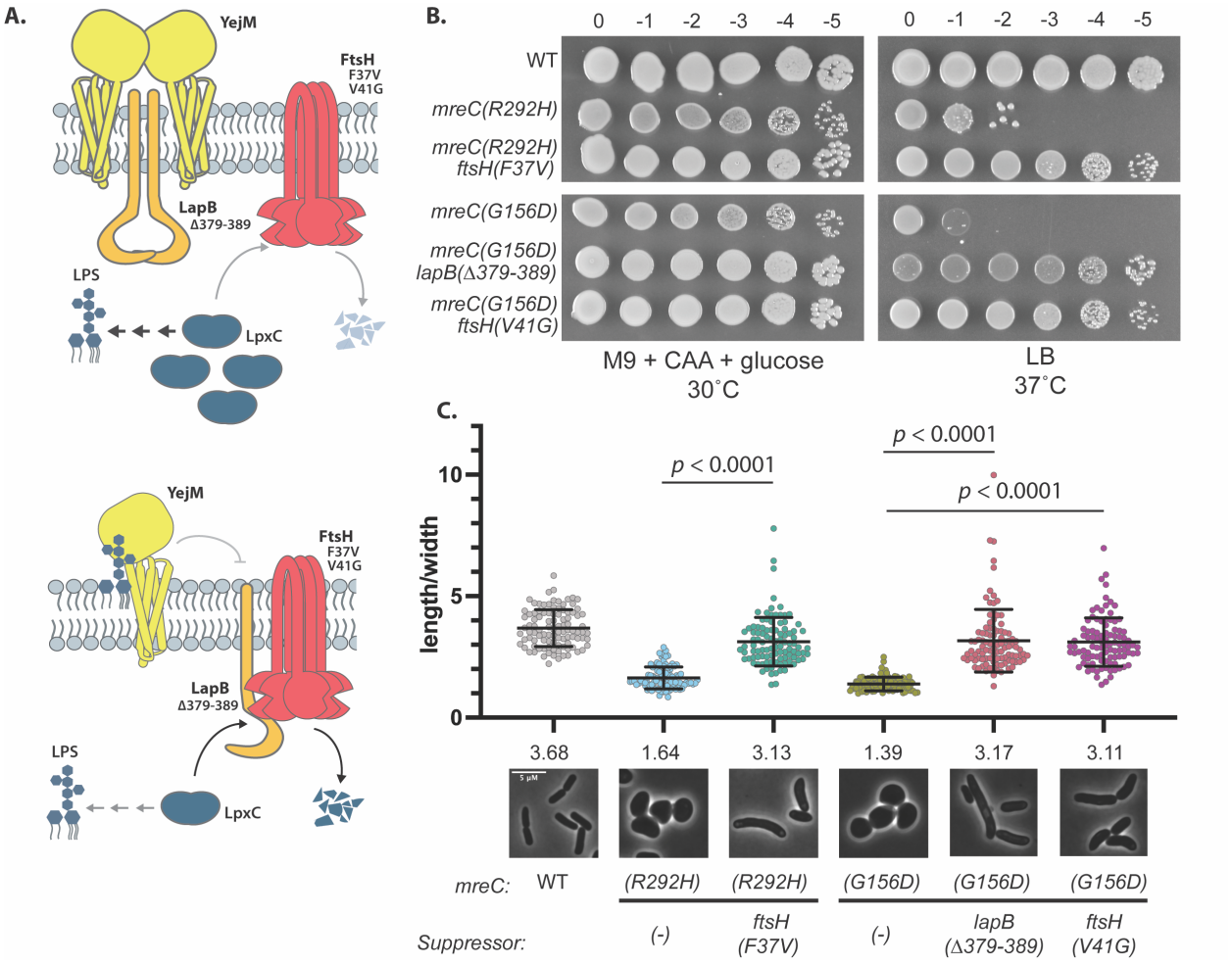

Figure 1: Mutations in factors involved in LpxC turnover rescue *mreC* hypomorphs. A. Schematic overview of LpxC regulation (suppressors mutations are noted below protein names). TOP: When LPS levels are low, YejM interacts with LapB, sequestering it from the FtsH protease, leading to the stabilization of LpxC and increased LPS synthesis. BOTTOM: When LPS levels are high, LPS accumulates in the outer leaflet of the inner membrane. YejM binds to LPS, allowing LapB to interact with FtsH and target LpxC for degradation, reducing LPS synthesis. **B**. WT (HC555), *mreC(R292H)* (PR5), *mreC(R292H) ftsH(V37G)* (PR82), *mreC(G156D)* (PR30), *mreC(G156D) lapB(Δ379-389)* (PR86), *mreC(G156D) ftsH(V41G)* (PR88) were cultured for 24 hours in minimal medium (M9 + CAA + glu) at 30˚C. Cultures were then normalized to OD_{600}= 1 and serially diluted and spotted onto LB and M9 + CAA + glu plates. LB plates were incubated for 16 hours at 37˚C and M9 plates were incubated for 40 hours at 30˚C. Dilution factors are indicated above the spot dilutions. **C**. Micrographs of WT (HC555), *mreC(R292H)* (PR5), *mreC(R292H) ftsH(V37G)* (PR82), *mreC(G156D)* (PR30), *mreC(G156D) lapB(Δ379-389)* (PR86), *mreC(G156D) ftsH(V41G)* (PR88). Strains were grown overnight in minimal

medium (M9 + CAA + glu) at 30˚C. Overnight cultures were then back diluted to OD_{600} = 0.05 in minimal medium and incubated shaking at 30˚C until OD_{600} = 0.3-0.4. Cells were then spun down and resuspended in LB to an OD_{600} of 0.025 and incubated at 37˚C until OD_{600} =0.3-0.4. Cells were then fixed and imaged. Aspect ratios were analyzed using the FIJI plugin MicrobeJ (70). Scale bar = 5 µm. n= 100 cells per group. Statistical significance determined using an Unpaired t test with Welch's correction (not assuming equal SDs).

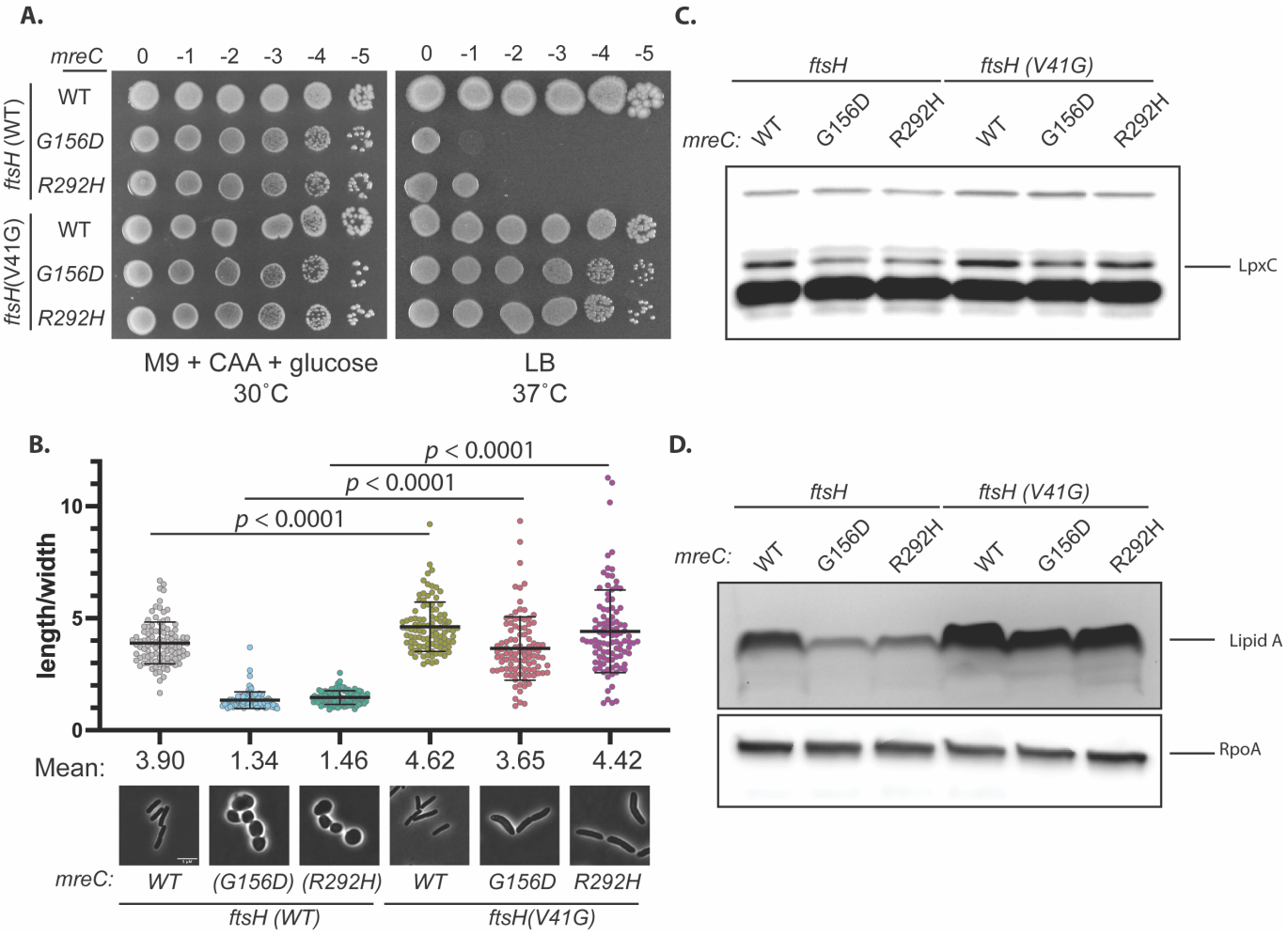

Figure 2: *FtsH(V41G)* increases LpxC and LPS levels in *mreC* hypomorphs. A. Cultures of WT(EMF196), *mreC(G156D)* (EMF197), *mreC(R292H)* (PR109), *ftsH(V41G)* (EMF199), *mreC(G156D) ftsH(V41G)* (PR111), *mreC(R292H) ftsH(V41G)* (PR110) were incubated in M9 + CAA + glu at 30˚C for 24 hours. Cultures were diluted and plated as in **Fig. 1**. **B**. Cultures of the strains listed in (A) were diluted to OD_{600} = 0.05 in M9 + CAA + glu and incubated at 30˚C until OD_{600} = 0.2-0.3. Cultures were gently spun down and resuspended in LB to an OD_{600} = 0.025 and incubated at 37˚C until OD =0.2-0.3. Cells were fixed and imaged (see methods). Aspect ratios were analyzed using the FIJI plugin MicrobeJ (70). Scale bar = 5 µm. n= 100 cells per group. Statistical significance was determined as in **Fig. 1**. **C**. Cultures of the strains listed in (A) were grown as described in (B) and an immunoblot for LpxC was performed. **D**. Cultures of the strains listed in (A) were grown as described in (B) and analyzed via silver stain for lipid A (top). Samples were normalized to total protein and an immunoblot for RpoA was performed to serve as a loading control.

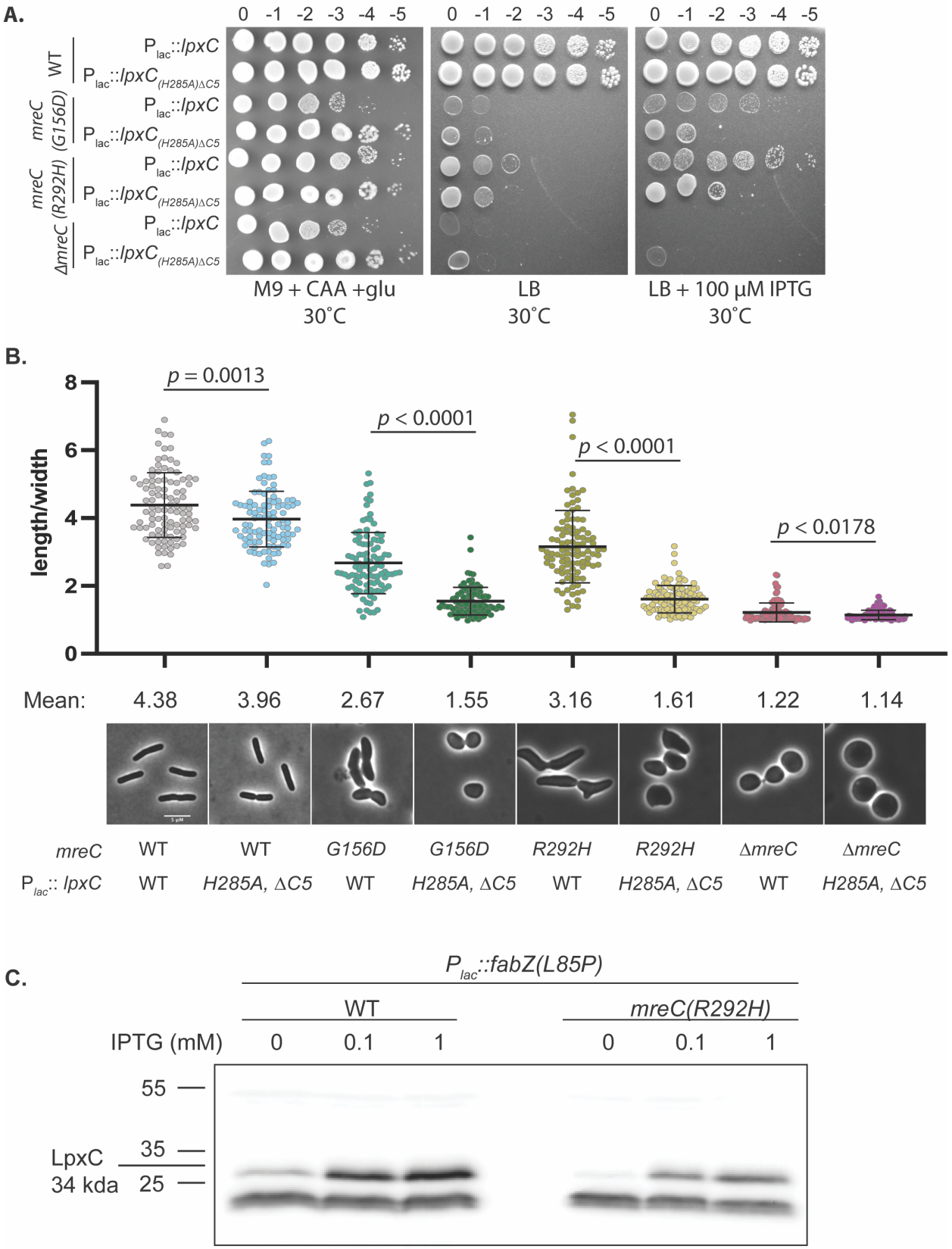

Figure 3: The overexpression of *lpxC* restores growth and partially restores shape to *mreC* hypermorphs. A. WT (HC555), *mreC(G156D)* (PR30), *mreC(R292H)* (PR5), and Δ*mreC* (EMF150) expressing WT *lpxC* (pPR111) or *lpxC(H285A)ΔC5* (pPR115) from an IPTG-inducible plasmid were

cultured for 24 hours at 30˚C in M9 + CAA + glu. Cultures were diluted and plated on the indicated media as in **Fig. 1**. All plates contained chloramphenicol. M9 plates were incubated at 30˚C for 40 hours and LB plates were incubated at 30˚C for 24 hours. **B**. The strains listed in (A) were grown for 24 hours at 30˚C in M9 + CAA + glu + CM. Cultures were diluted to OD_{600} = 0.025 in M9 + CAA + glu + CM + 50 μM IPTG and incubated at 30˚C until OD_{600} = 0.2-0.3. Cells were gently pelleted and resuspended in LB + CM + 50 μM IPTG and grown at 37˚C for 1 hour 45 min. Cells were then fixed and imaged (materials and methods). Aspect ratios were analyzed using the FIJI plugin MicrobeJ (70). Scale bar = 5 μm. n= 100 cells per group. Statistical significance was determined as in **Fig. 1**. **C**. Immunoblot for LpxC. Cell lysates of WT (HC555) and *mreC(R292H)* (PR5) cells harboring plasmids expressing *fabZ(L85P)* from an IPTG-inducible promoter (pEMF137) were cultured in M9 + CAA + glu + CM at 30˚C for 24 hrs. Cultures were then diluted to OD_{600} = 0.025 in M9 + CAA + glu + CM and grown at 30˚C until OD_{600} = 0.2-0.3. Cells were gently pelleted and resuspended in LB + CM +/- IPTG as indicated and grown at 37˚C for 2 hours and were subsequently harvested via centrifugation and processed for immunoblotting.

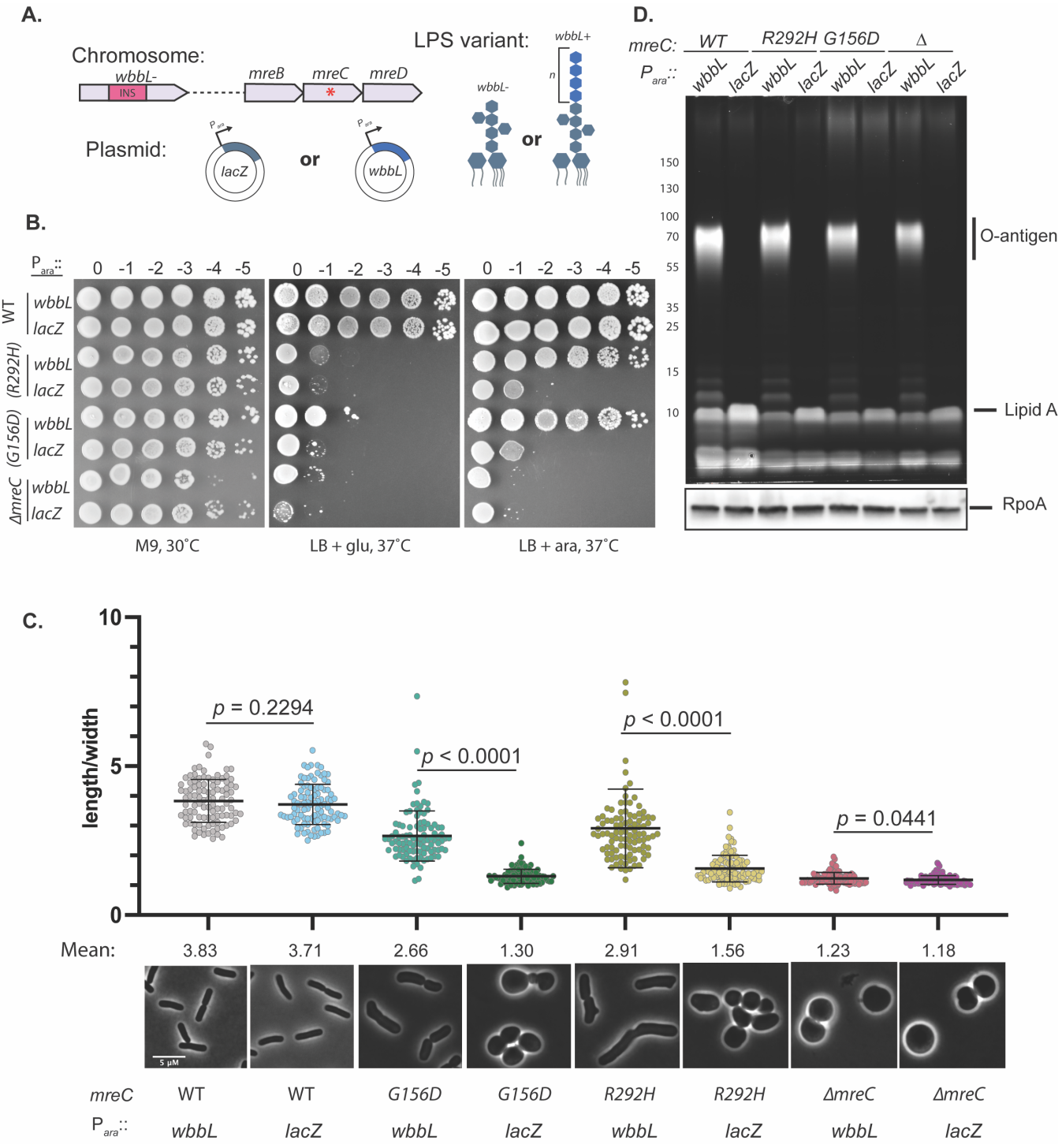

Figure 4: Synthesis of O-antigen-modified LPS suppressed the growth and shape defects of *mreC* hypomorphs. A. Schematic of strains. The *wbbL* gene in *E. coli* K-12 is disrupted by an insertion element, preventing the synthesis of O-antigen. *wbbL* is expressed *in trans* from an arabinose (ara)-inducible promoter, restoring O-antigen synthesis. *lacZ* is expressed as a control. **B**. WT (HC555), *mreC(R292H)* (PR5), *mreC(G156D)* (PR30), and Δ*mreC* (EMF150) expressing *wbbL* (pEMF130) or *lacZ* (pEMF134) from an arabinose-inducible promoter were incubated for 24 hours in M9 + CAA + glu + tet at 30˚C. Cultures were diluted and plated on the indicated media as in **Fig. 1**. **C**. The strains listed in (A) were grown for 24 hours in M9 + CAA + glu + tet at 30˚C and diluted to OD_{600} = 0.05 in M9 +CAA + ara + tet for 3 hours at 30˚C. After 3 hours, the cultures were gently pelleted and resuspended in LB + tet +

ara. Cells were grown for 2 hrs at 37˚C. Cells were then fixed and imaged (materials and methods). Aspect ratios were analyzed using the FIJI plugin MicrobeJ (70). Scale bar = 5 μm. n= 100 cells per group. Statistical significance was determined as in **Fig. 1**. **D**. Proemerald Q stain of LPS. The strains listed in (A) were grown as described in (B). Cell lysates were prepared and LPS was analyzed via promerald Q straining.

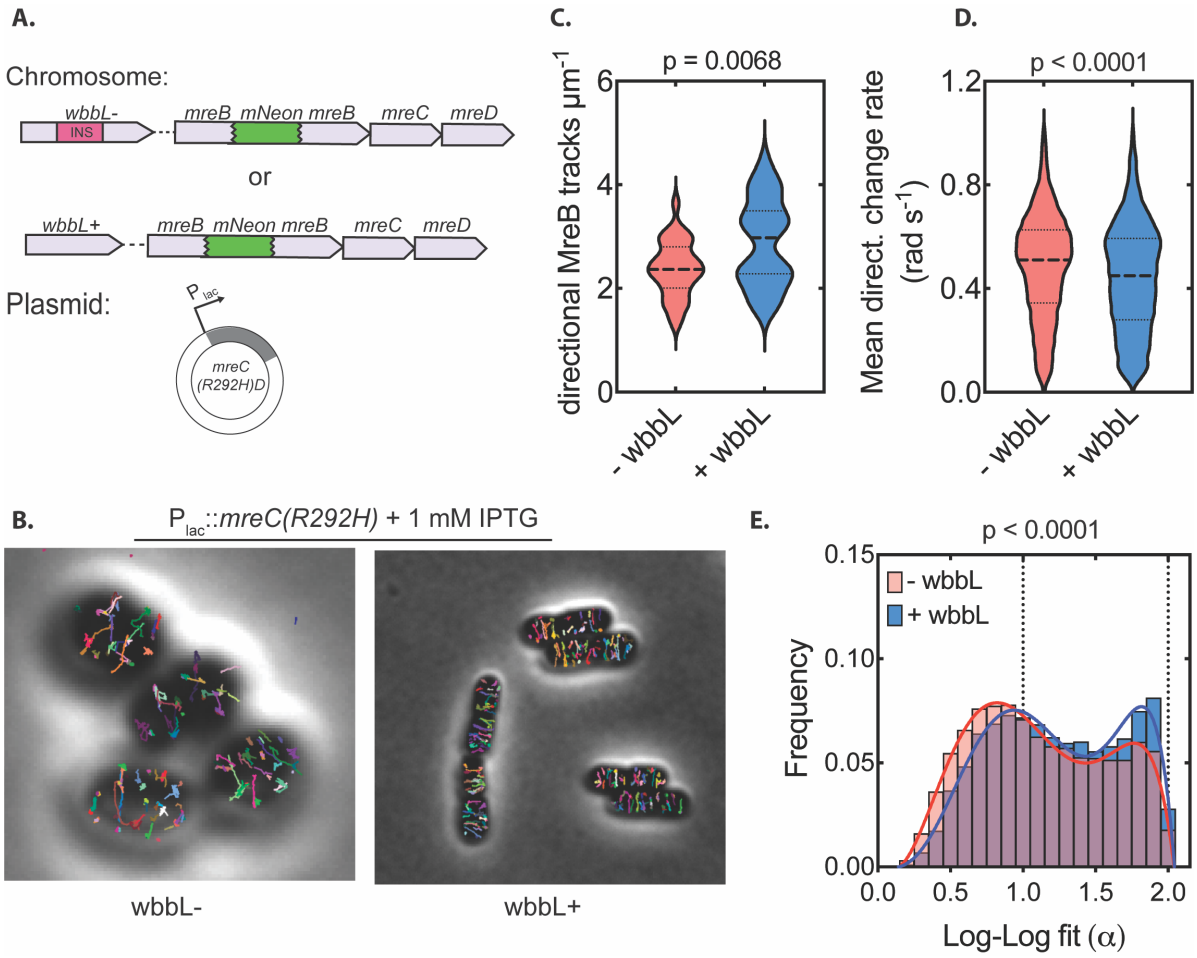

Figure 5: MreB dynamics upon rod system inactivation by *mreC(R292H)* in cells with or without O-antigen. A. Schematic of strains. ^{SW}*mreB-mNeon* cells harbor either *wbbL*(INS) (AV007) or *wbbL*+ (EMF210) at the native chromosomal locus, resulting in cells without or with O-antigen-modified LPS, respectively. *mreC(R292H)D* is expressed in trans from an IPTG-inducible promoter (pMS9). **B**. *wbbL(INS)* (AV007) or *wbbL*+ (EMF210) cells expressing *mreC(R292H)D* (pMS9). Individual traces of MreB tracks were mapped using the TrackMate feature of FIJI (72, 75). Each track is indicated in different color. **C**. Violin plot of the number of directional MreB tracks per cell area in cells with (EMF210) and without O-antigen (AV007) expressing *mreC(R292H)D* (pMS9). (n= 30 cells (AV007), n=31 cells (EMF210)) **D**. Violin plot of the mean directional change rate of MreB tracks in *wbbL*(-) and *wbbL* (+) cells (n=10214 tracks (AV007), n= 9162 tracks (EMF210)) **E.** Histogram of the log-log fit (α) values of Individual MreB traces in cells with (EMF210) and without O-antigen (AV007) expressing *mreC(R292H)D* (pMS9). (n=18618 tracks (AV007), n=15070 tracks (EMF210)).

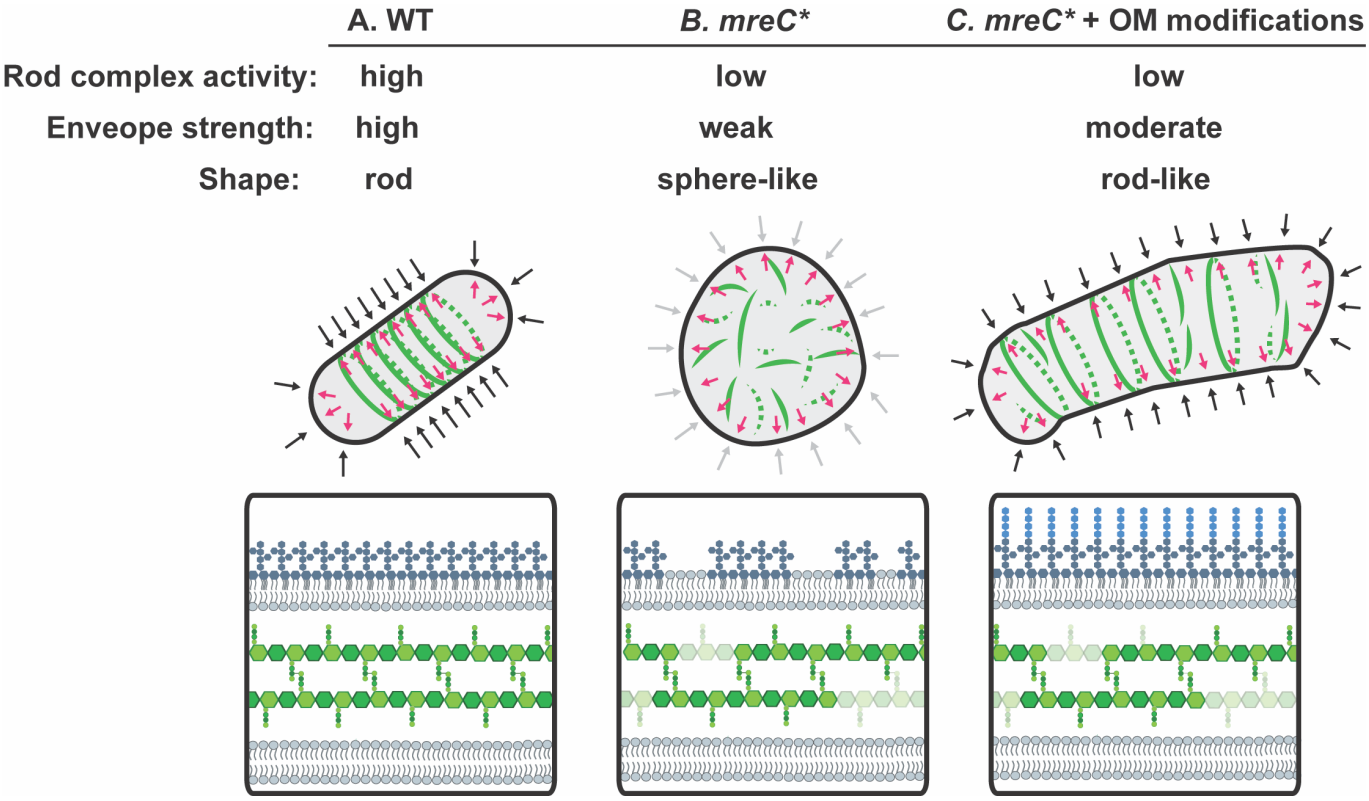

Figure 6: Interventions that strength the outer membrane restore shape to Rod system hypomorphs. A. In wildtype cells, the internal turgor pressure of the cell is countered by the combined mechanical strength of the cell wall and the outer membrane. The Rod complex is fully functional and is orientated by MreB, which aligns along the greatest principle curvature to ensure synthesis perpendicular to the long axis of the cell. **B.** In hypomorphic *mreC* mutants (*mreC**), the Rod complex is not able to synthesize sufficient peptidoglycan or LPS, weakening the envelope and leading to loss of rod shape. The cells no longer form a clearly defined long axis, causing MreB filaments to misalign. The reduced Rod complex activity in these mutants is therefore not properly oriented. **C.** When the mechanical strength of the outer membrane is increased, the cell envelope is sufficiently able to resist the internal turgor pressure of the cell to allow for the initiation and propagation of a rod shape by allowing MreB and limited PG synthesis by the Rod complex to properly orient.

REFERENCES

1. P. D. Rohs, T. G. Bernhardt, Growth and division of the peptidoglycan matrix. *Annu. Rev. Microbiol.* **75**, 315-336 (2021).
2. A. Typas, M. Banzhaf, C. A. Gross, W. Vollmer, From the regulation of peptidoglycan synthesis to bacterial growth and morphology. *Nat. Rev. Microbiol.* **10**, 123 (2012).
3. E. R. Rojas *et al.*, The outer membrane is an essential load-bearing element in Gram-negative bacteria. *Nature* **559**, 617 (2018).
4. J.-V. Höltje, Growth of the stress-bearing and shape-maintaining murein sacculus of *Escherichia coli*. *Microbiol. Mol. Biol. Rev.* **62**, 181-203 (1998).

5. E. Sauvage, F. Kerff, M. Terrak, J. A. Ayala, P. Charlier, The penicillin-binding proteins: structure and role in peptidoglycan biosynthesis. *FEMS Microbiol. Rev.* **32**, 234-258 (2008).
6. A. J. Meeske *et al.*, SEDS proteins are a widespread family of bacterial cell wall polymerases. *Nature* **537**, 634-638 (2016).
7. H. Cho *et al.*, Bacterial cell wall biogenesis is mediated by SEDS and PBP polymerase families functioning semi-autonomously. *Nat. Microbiol.* **1**, 1-8 (2016).
8. K. Emami *et al.*, RodA as the missing glycosyltransferase in *Bacillus subtilis* and antibiotic discovery for the peptidoglycan polymerase pathway. *Nat. Microbiol.* **2**, 1-9 (2017).
9. A. Taguchi *et al.*, FtsW is a peptidoglycan polymerase that is functional only in complex with its cognate penicillin-binding protein. *Nat. Microbiol.* **4**, 587-594 (2019).
10. P. D. Rohs *et al.*, A central role for PBP2 in the activation of peptidoglycan polymerization by the bacterial cell elongation machinery. *PLoS Genet.* **14**, e1007726 (2018).
11. F. O. Bendezú, P. A. De Boer, Conditional lethality, division defects, membrane involution, and endocytosis in mre and mrd shape mutants of *Escherichia coli. J. Bacteriol.* **190**, 1792-1811 (2008).
12. F. O. Bendezú, C. A. Hale, T. G. Bernhardt, P. A. De Boer, RodZ (YfgA) is required for proper assembly of the MreB actin cytoskeleton and cell shape in *E. coli*. *The EMBO journal* **28**, 193-204 (2009).
13. S. A. Alyahya *et al.*, RodZ, a component of the bacterial core morphogenic apparatus. *Proc. Natl. Acad. Sci.* U.S.A. **106**, 1239-1244 (2009).
14. T. Kruse, J. Bork-Jensen, K. Gerdes, The morphogenetic MreBCD proteins of *Escherichia coli* form an essential membrane-bound complex. *Mol. Microbiol.* **55**, 78-89 (2005).
15. M. Leaver, J. Errington, Roles for MreC and MreD proteins in helical growth of the cylindrical cell wall in *Bacillus subtilis*. *Mol. Microbiol.* **57**, 1196-1209 (2005).
16. R. M. Morgenstein *et al.*, RodZ links MreB to cell wall synthesis to mediate MreB rotation and robust morphogenesis. *Proc. Natl. Acad. Sci.* U.S.A. **112**, 12510-12515 (2015).
17. D. Shiomi, M. Sakai, H. Niki, Determination of bacterial rod shape by a novel cytoskeletal membrane protein. *The EMBO journal* **27**, 3081-3091 (2008).
18. M. Wachi, M. Matsuhashi, Negative control of cell division by *mreB*, a gene that functions in determining the rod shape of *Escherichia coli* cells. *J. Bacteriol.* **171**, 3123-3127 (1989).
19. R. A. Daniel, J. Errington, Control of cell morphogenesis in bacteria: two distinct ways to make a rod-shaped cell. *Cell* **113**, 767-776 (2003).
20. J. Domínguez-Escobar *et al.*, Processive movement of MreB-associated cell wall biosynthetic complexes in bacteria. *Science* **333**, 225-228 (2011).
21. E. C. Garner, Toward a mechanistic understanding of bacterial rod shape formation and regulation. *Annu. Rev. Cell Dev. Biol.* **37**, 1-21 (2021).
22. S. Van Teeffelen *et al.*, The bacterial actin MreB rotates, and rotation depends on cell-wall assembly. *Proc. Natl. Acad. Sci.* U.S.A. **108**, 15822-15827 (2011).
23. P. D. Rohs *et al.*, Identification of potential regulatory domains within the MreC and MreD components of the cell elongation machinery. *J. Bacteriol.* **203**, e00493-00420 (2021).
24. X. Liu, J. Biboy, E. Consoli, W. Vollmer, T. den Blaauwen, MreC and MreD balance the interaction between the elongasome proteins PBP2 and RodA. *PLoS Genet.* **16**, e1009276 (2020).
25. G. Özbaykal *et al.*, The transpeptidase PBP2 governs initial localization and activity of the major cell-wall synthesis machinery in *E. coli. Elife* **9**, e50629 (2020).
26. G. Klein, N. Kobylak, B. Lindner, A. Stupak, S. Raina, Assembly of lipopolysaccharide in *Escherichia coli* requires the essential LapB heat shock protein. *J. Biol. Chem.* **289**, 14829-14853 (2014).

27. S. Mahalakshmi, M. Sunayana, L. SaiSree, M. Reddy, yciM is an essential gene required for regulation of lipopolysaccharide synthesis in *Escherichia coli*. *Mol. Microbiol.* **91**, 145-157 (2014).
28. K. Ito, Y. Akiyama, Cellular functions, mechanism of action, and regulation of FtsH protease. *Annu. Rev. Microbiol.* **59**, 211-231 (2005).
29. T. Ogura *et al.*, Balanced biosynthesis of major membrane components through regulated degradation of the committed enzyme of lipid A biosynthesis by the AAA protease FtsH (HflB) in *Escherichia coli*. *Mol. Microbiol.* **31**, 833-844 (1999).
30. S. Shu, W. Mi, Regulatory mechanisms of lipopolysaccharide synthesis in Escherichia coli. *Nat. Commun.* **13**, 1-11 (2022).
31. M. S. Anderson, A. D. Robertson, I. Macher, C. R. Raetz, Biosynthesis of lipid A in *Escherichia coli*: identification of UDP-3-O-[(R)-3-hydroxymyristoyl]-. alpha.-D-glucosamine as a precursor of UDP-N2, O3-bis [(R)-3-hydroxymyristoyl]-. alpha.-D-glucosamine. *Biochemistry* **27**, 1908-1917 (1988).
32. K. Young *et al.*, The envA permeability/cell division gene of *Escherichia coli* encodes the second enzyme of lipid A biosynthesis. UDP-3-O-(R-3-hydroxymyristoyl)-N-acetylglucosamine deacetylase. *J. Biol. Chem.* **270**, 30384-30391 (1995).
33. M. B. Cian, N. P. Giordano, R. Masilamani, K. E. Minor, Z. D. Dalebroux, Salmonella enterica serovar Typhimurium use PbgA/YejM to regulate lipopolysaccharide assembly during bacteremia. *Infect. Immun.*, IAI. 00758-00719 (2019).
34. T. Clairfeuille *et al.*, Structure of the essential inner membrane lipopolysaccharide–PbgA complex. *Nature* **584**, 479-483 (2020).
35. E. M. Fivenson, T. G. Bernhardt, An Essential Membrane Protein Modulates the Proteolysis of LpxC to Control Lipopolysaccharide Synthesis in *Escherichia coli. mBio* **11**, e00939-00920 (2020).
36. R. L. Guest, D. Samé Guerra, M. Wissler, J. Grimm, T. J. Silhavy, YejM Modulates Activity of the YciM/FtsH Protease Complex To Prevent Lethal Accumulation of Lipopolysaccharide. *mBio* **11**, e00598-00520 (2020).
37. D. Nguyen, K. Kelly, N. Qiu, R. Misra, YejM Controls LpxC Levels by Regulating Protease Activity of the FtsH/YciM Complex of *Escherichia coli*. *J. Bacteriol.* **202**, e00303-00320 (2020).
38. D. Biernacka, P. Gorzelak, G. Klein, S. Raina, Regulation of the first committed step in lipopolysaccharide biosynthesis catalyzed by LpxC requires the essential protein LapC (YejM) and HslVU protease. *Int. J. Mol. Sci.* **21**, 9088 (2020).
39. F. Führer, S. Langklotz, F. Narberhaus, The C-terminal end of LpxC is required for degradation by the FtsH protease. *Mol. Microbiol.* **59**, 1025-1036 (2006).
40. J. E. Jackman, C. R. Raetz, C. A. Fierke, Site-directed mutagenesis of the bacterial metalloamidase UDP-(3-O-acyl)-N-acetylglucosamine deacetylase (LpxC). Identification of the zinc binding site. *Biochemistry* **40**, 514-523 (2001).
41. R. J. Heath, C. O. Rock, Roles of the FabA and FabZ β-hydroxyacyl-acyl carrier protein dehydratases in *Escherichia coli* fatty acid biosynthesis. *J. Biol. Chem.* **271**, 27795-27801 (1996).
42. M. Schäkermann, S. Langklotz, F. Narberhaus, FtsH-mediated coordination of lipopolysaccharide biosynthesis in *Escherichia coli* correlates with the growth rate and the alarmone (p) ppGpp. *J. Bacteriol.* **195**, 1912-1919 (2013).
43. A. L. McClerren *et al.*, A slow, tight-binding inhibitor of the zinc-dependent deacetylase LpxC of lipid A biosynthesis with antibiotic activity comparable to ciprofloxacin. *Biochemistry* **44**, 16574-16583 (2005).
44. A. W. Barb *et al.*, Inhibition of lipid A biosynthesis as the primary mechanism of CHIR-090 antibiotic activity in *Escherichia coli*. *Biochemistry* **46**, 3793-3802 (2007).

45. A. Emiola, S. S. Andrews, C. Heller, J. George, Crosstalk between the lipopolysaccharide and phospholipid pathways during outer membrane biogenesis in *Escherichia coli*. *Proc. Natl. Acad. Sci.* U.S.A. **113**, 3108-3113 (2016).
46. E. Bi, J. Lutkenhaus, Cell division inhibitors SulA and MinCD prevent formation of the FtsZ ring. *J. Bacteriol.* **175**, 1118-1125 (1993).
47. S. C. Cordell, E. J. Robinson, J. Löwe, Crystal structure of the SOS cell division inhibitor SulA and in complex with FtsZ. *Proc. Natl. Acad. Sci.* U.S.A. **100**, 7889-7894 (2003).
48. A. Mukherjee, C. Cao, J. Lutkenhaus, Inhibition of FtsZ polymerization by SulA, an inhibitor of septation in *Escherichia coli*. *Proc. Natl. Acad. Sci.* U.S.A. **95**, 2885-2890 (1998).
49. H. Cho, T. Uehara, T. G. Bernhardt, Beta-lactam antibiotics induce a lethal malfunctioning of the bacterial cell wall synthesis machinery. *Cell* **159**, 1300-1311 (2014).
50. C. Whitfield, M. S. Trent, Biosynthesis and export of bacterial lipopolysaccharides. *Annu. Rev. Biochem.* **83**, 99-128 (2014).
51. X. Rubirés *et al.*, A gene (wbbL) from Serratia marcescens N28b (O4) complements the rfb-50 mutation of Escherichia coli K-12 derivatives. *J. Bacteriol.* **179**, 7581-7586 (1997).
52. B. W. Simpson, M. S. Trent, Pushing the envelope: LPS modifications and their consequences. *Nat. Rev. Microbiol.* **17**, 403-416 (2019).
53. L. E. Bretscher, M. T. Morrell, A. L. Funk, C. S. Klug, Purification and characterization of the L-Ara4N transferase protein ArnT from *Salmonella typhimurium*. *Protein Expr. Purif.* **46**, 33-39 (2006).
54. M. S. Trent, A. A. Ribeiro, S. Lin, R. J. Cotter, C. R. Raetz, An Inner Membrane Enzyme in *Salmonella and Escherichia coli* That Transfers 4-Amino-4-deoxy-l-arabinose to Lipid A: INDUCTION IN POLYMYXIN-RESISTANT MUTANTS AND ROLE OF A NOVEL LIPID-LINKED DONOR* 210. *J. Biol. Chem.* **276**, 43122-43131 (2001).
55. S. Hussain *et al.*, MreB filaments align along greatest principal membrane curvature to orient cell wall synthesis. *Elife* **7**, e32471 (2018).
56. M. S. Anderson, C. Raetz, Biosynthesis of lipid A precursors in *Escherichia coli*. A cytoplasmic acyltransferase that converts UDP-N-acetylglucosamine to UDP-3-O-(R-3-hydroxymyristoyl)-N-acetylglucosamine. *J. Biol. Chem.* **262**, 5159-5169 (1987).
57. D. N. Crowell, M. S. Anderson, C. Raetz, Molecular cloning of the genes for lipid A disaccharide synthase and UDP-N-acetylglucosamine acyltransferase in *Escherichia coli*. *J. Bacteriol.* **168**, 152-159 (1986).
58. J. Marquardt, D. Siegele, R. Kolter, C. Walsh, Cloning and sequencing of *Escherichia coli* murZ and purification of its product, a UDP-N-acetylglucosamine enolpyruvyl transferase. *J. Bacteriol.* **174**, 5748-5752 (1992).
59. V. Braun, K. Rehn, Chemical characterization, spatial distribution and function of a lipoprotein (murein-lipoprotein) of the *E. coli* cell wall: the specific effect of trypsin on the membrane structure. *Eur. J. Biochem.* **10**, 426-438 (1969).
60. M. Inouye, J. Shaw, C. Shen, The assembly of a structural lipoprotein in the envelope of *Escherichia coli*. *J. Biol. Chem.* **247**, 8154-8159 (1972).
61. H. Suzuki *et al.*, Murein-lipoprotein of *Escherichia coli*: a protein involved in the stabilization of bacterial cell envelope. *Mol. Gen. Genet.* **167**, 1-9 (1978).
62. G. Mamou *et al.*, Peptidoglycan maturation controls outer membrane protein assembly. *Nature* **606**, 953-959 (2022).
63. J. Sun, S. T. Rutherford, T. J. Silhavy, K. C. Huang, Physical properties of the bacterial outer membrane. *Nat. Rev. Microbiol.*, 1-13 (2021).

64. A. Formstone, J. Errington, A magnesium-dependent mreB null mutant: implications for the role of mreB in Bacillus subtilis. *Mol. Microbiol.* **55**, 1646-1657 (2005).
65. H. Rogers, P. Thurman, R. Buxton, Magnesium and anion requirements of rodB mutants of Bacillus subtilis. *J. Bacteriol.* **125**, 556-564 (1976).
66. J. A. Buss *et al.*, Pathway-directed screen for inhibitors of the bacterial cell elongation machinery. *Antimicrob. Agents Chemother.* **63**, e01530-01518 (2019).
67. J. Miller (1972) Experiments in molecular genetics. Cold Spring Laboratory Press. (Cold Spring Harbor, NY).
68. C.-M. Tsai, C. E. Frasch, A sensitive silver stain for detecting lipopolysaccharides in polyacrylamide gels. *Anal. Biochem.* **119**, 115-119 (1982).
69. J. Schindelin *et al.*, Fiji: an open-source platform for biological-image analysis. *Nat. methods* **9**, 676-682 (2012).
70. A. Ducret, E. M. Quardokus, Y. V. Brun, MicrobeJ, a tool for high throughput bacterial cell detection and quantitative analysis. *Nat. Microbiol.* **1**, 1-7 (2016).
71. P. P. Navarro *et al.*, Cell wall synthesis and remodelling dynamics determine division site architecture and cell shape in *Escherichia coli*. *Nat. Microbiol.* **7**, 1621-1634 (2022).
72. J.-Y. Tinevez *et al.*, TrackMate: An open and extensible platform for single-particle tracking. *Methods* **115**, 80-90 (2017).
73. N. Tarantino *et al.*, TNF and IL-1 exhibit distinct ubiquitin requirements for inducing NEMO–IKK supramolecular structures. *J. Cell Biol.* **204**, 231-245 (2014).
74. E. C. Garner *et al.*, Coupled, circumferential motions of the cell wall synthesis machinery and MreB filaments in *B. subtilis*. *Science* **333**, 222-225 (2011).
75. D. Ershov *et al.*, TrackMate 7: integrating state-of-the-art segmentation algorithms into tracking pipelines. *Nat. Methods*, 1-4 (2022).

Supporting Information for:

A role for the Gram-negative outer membrane in bacterial shape determination

Authors: Elayne M. Fivenson[1], Patricia D.A. Rohs[1], Andrea Vettiger[1], Marios F. Sardis[1], Grasiela Torres[1], Alison Forchoh[1], and Thomas G. Bernhardt[1,2*]

Affiliations:
[1]Department of Microbiology, Blavatnik Institute, Harvard Medical School, Boston, MA 02115.
[2]Howard Hughes Medical Institute, Boston, United States.

***To whom correspondence should be addressed**.
Thomas G. Bernhardt, Ph.D.
Harvard Medical School
Department of Microbiology
Boston, Massachusetts 02115
e-mail: thomas_bernhardt@hms.harvard.edu

Supporting text

Molecular biology

The polymerase chain reaction (PCR) was carried out using Q5 High fidelity polymerase (New England Biolabs) or GoTaq green master mix (Promega) following manufacturer's instructions. PCR products were purified using the PCR clean up kit from Qiagen or CWBiosciences. Plasmids were isolated using the Miniprep Kit from Qiagen or the plasmid purification kit from CWBiosciences.

Strain construction details

PR82
See supplementary table 1 and Methods

PR86
See supplementary table 1 and Methods

PR88
See supplementary table 1 and Methods

EMF196
The *yrdE-kan* allele from strain HC555 was transduced into strain PR103 by P1-mediated transduction. Transductants were selected on LB + kan25 and confirmed for the yrdE-kan allele via PCR.

PR103
The *leuU-cat-yhbX* allele from strain PR90 was transduced into MG1655 by P1-mediated transduction. Transductants were selected on LB + CM25.

PR90
A chloramphenicol resistance cassette was introduced to strain TB10 between *leuU* and *yhbX* (linked to *ftsH*) by lambda red recombineering. A PCR product amplified from pKD3 was generated using Primers leuU-yhbX_P2_F (ACCTTGAAACGATGGTGCCGGTACGCCTTAGTTATAAATTCATATGAATATCCTCCTTAG) and leuU-yhbX_P1_R (TTGACACAATAAAGTGCCAATTATGTCAGTAGAAGGGAAAGTGTAGGCTGGAGCTGCTTC) and electroporated into strain TB10 following the protocol for strain DY329 described previously(1).

EMF197
The *yrdE-kan* marker linked to the *mreC(G156D)* allele from strain PR30/pTB63 was transduced into strain PR103 via P1-mediated transduction. Transductants were selected on M9 + CAA + glu + kan25. The *mreC(G156D)* allele was confirmed via sequencing.

EMF199
The *yrdE-kan* allele from strain HC555 was transduced into strain PR104 by P1-mediated transduction. Transductants were selected on LB + kan25 and confirmed for the *yrdE-kan* allele via PCR.

PR104
The *leuU-cat-yhbX* allele linked to *ftsH(V41G)* from strain PR96 was transduced into MG1655 via P1-mediated transduction. Transductants were selected on LB + CM25 and confirmed for the *ftsH(V41G*) allele via sequencing.

PR96
A chloramphenicol resistance cassette was introduced to strain PR88 between *leuU* and *yhbX* (linked to *ftsH*) by lambda red recombineering with pKD46 plasmid following the protocol described previously (2) . A PCR product amplified from pKD3 using primers leuU-yhbX_P2_F (ACCTTGAAACGATGGTGCCGGTACGCCTTAGTTATAAATTCATATGAATATCCTCCTTAG) and leuU-yhbX_P1_R (TTGACACAATAAAGTGCCAATTATGTCAGTAGAAGGGAAAGTGTAGGCTGGAGCTGCTTC) and electroporated into strain PR88/pKD46.

PR109
The *yrdE-kan* marker linked to *mreC(R292H)* from strain PR5/pTB63 was transduced into strain PR103 by P1-mediated transduction. Transductants were select on M9 + CAA + glu + kanamycin.

PR111
The *yrdE-kan* marker linked to the *mreC(G156D*) allele from strain PR30/pTB63 was transduced into strain PR104 via P1-mediated transduction. Transductants were select on M9 + CAA + glu + kanamycin. The *mreC(G156D*) allele was confirmed via sequencing

PR110
The *yrdE-kan* marker linked to *mreC(R292H)* from strain PR5/pTB63 was transduced into strain PR104 by P1-mediated transduction. Transductants were select on M9 + CAA + glu + kanamycin. The *mreC(R292H*) allele was confirmed via sequencing.

EMF150
The Δ*mreC::kan* allele from strain MT4/pTB63 was transduced into MG1655 via P1-mediated transduction. Transductants were select on M9 + CAA + glu + kanamycin.

AV007
The chloramphenicol resistance cassette in strain JAB593 was cured using pcp20 as described previously (3).

EMF210
The *wbbL+* allele linked to a kanamycin resistance cassette from strain NR2528 was transduced into AV007 by P1-mediated transduction. Transductants were selected on LB + kan25 and confirmed via PCR.

EMF52(attHKHC859)

The *ftsH(V41G)* allele linked to the *leuU*-cat- *yhbX* marker was transduced from strain PR96 into strain HC533(attHKHC859) by P1-mediated transduction. Transductants were selected on LB + CM25 and the *ftsH(V41G)* allele was confirmed via sequencing.

EMF53(attHKHC859)
The *leuU*-cat-*yhbX* marker was transduced from strain PR90 into strain HC533(attHKHC859) by P1-mediated transduction. Transductants were selected on LB + CM25 and confirmed via PCR.

EMF212
MG1655 x P1(EMF211)
The kanamycin resistance cassette downstream of *wbbL(INS*) was transduced form EMF211 into MG1655 by P1-mediated transduction. Transductants were selected on LB + kan25 and confirmed by PCR.

EMF211
A kanamycin resistance cassette introduced to strain TB10 downstream of *wbbL(INS)* by lambda red recombineering. A PCR product amplified from pKD4 was generated using primers wbbL_kan_F (TCGCAACTTTGATCGAATTTCATCAGTTTTTCACCCGTAAGCGATTGTGTAGGCTGGAGC) and wbbL_kan_R (ATAAATAGCTTATCCATGCTTATATGCTTACGGCTTTATACTATTCCGAAGTTCCTATTC) and electroporated into strain TB10 following the protocol for strain DY329 described previously(1).

EMF214
The *wbbL*+ allele linked to a kanamycin resistance cassette from strain NR2528 was transduced into PR134 by P1-mediated transduction. Transductants were selected on M9 + CAA + glu + kan and confirmed via PCR.

Plasmid Construction details

pPR112
The nativeRBS_lpxC insert was PCR amplified from E. coli K12 genomic DNA using forward primer LpxC_nativeRBS_XbaI5' (CCCCTCTAGATAATTTGGCGAGATAATACGATGATC) and reverse primer lpxC_3'truncation_HindIII (TGATAAGCTTATTAAGGCGCTTTGAAGGCCAACGG) resulting in an amplified PCR product of the nativeRBS and coding sequencing of lpxC lacking the 5 terminal amino acids. Primers contain xbaI and hindIII restriction sites, respectively. The PCR fragment was cloned into empty vector pPR66 using restriction enzymes xbaI and hindIII.

pPR115
pPR112 mutated with quickchange mutagenesis using primer lpxC_quickchange_H265A (TACCGCTTATAAATCCGGTGCTGCACTGAATAACAAACTG)

pEMF51
The *nativeRBS_fabZ(L85P)* insert was generated by amplifying the *fabZ* locus from strain EMF63 using primers xbaI_fabZ_F (ATCCTCTAGATGTCGTTTCTTATATTTTGACAGGAAGAG) and

hindIII_fabZ_R (TACCAAGCTTTCAGGCCTCCCGGCTACG). This PCR product was digested with restriction enzymes xbaI and hindIII and ligated into pNP140.

pEMF137
pEMF51 and pPR66 were digested with restriction enzymes xbaI and hindIII-HF. The *nativeRBS_fabZ(L85P)* insert from pEMF51 was ligated into the pPR66 vector.

pEMF112
The plasmids pNP146 and pPR111 were digested with restriction enzymes xbaI and hindIII-HF. The pNP146 vector backbone was ligated with the *nativeRBS_lpxC* insert from pPR111

pEMF131
A PCR product was generated by amplifying the *nativeRBS_ pbp2(L61R)rodA* insert from pPR122 using primers pEMF131_F (CAAATCTAGATAAGGGAGCTTTGAGTAG) and pEMF131_R (TGATAAGCTTATGCGCACCTCTTACACGCTTTTC). The resulting PCR product was digested with restriction enzymes xbaI and hindIII-HF and ligated into the vector backbone of pNP146.

pPR122
A PCR product was generated by amplifying the *pbp2(L61R)* allele from genomic DNA from strain PR39 using primers XbaI-pbpA (GCTATCTAGATAAGGGAGCTTTGAGTAGAAAACG) and HindIII-pbpA (GCTAAAGCTTTTTATTCGGATTATCCGTCATG). This PCR product was digested with restriction enzymes xbaI and hindIII and ligated into the vector backbone of pHC857.

pAF2
A PCR product was generated by amplifying the *arnT* locus from MG1655 gDNA using primers arnT_xbaI_F (CCCCTCTAGATTTAAGAAGGAGATATACATATGAAATCGGTACGTTACCTTATCGG) and arnT_hindIII_R (TGATAAGCTTATCATTTGGGACGATACTGAATCAGC) to generate the artificalRBS_arnT fragment which was then digested with restriction enzymes xbaI and hindIII and ligated into the pPR66 vector backbone.

pEMF130
wbbL amplified from gDNA from strain AAY1using prmers wbbL XbaI-RBS-NdeI5': (TCTAGATTAAGAAGGAGATATACATATGGTATATATAATAATCGTTTCCCACGG) and wbbL_HindIII_Rev (AAGCTTTTACGGGTGAAAAACTGATGAAATTCGATCAAAGTTGCG). The resulting PCR product (xbaI-artificialRBS-wbbL) was cloned into vector pNP146 using restriction enzymes xbaI and hindIII.

pEMF134
lacZ was amplified from MG1655 gDNA using primers xbaI_strongRBS_lacZ (ATCCTCTAGACTTTAAGAAGGAGATATACCATGACCATGATTACGGATTCACTGG) and hindIII_lacZ_R (TGATAAGCTTATTATTTTTGACACCAGACCAACTGGTAATG). The resulting PCR product (xbaI-artificialRBS-lacZ) was cloned into vector pNP146 using restriction enzymes xbaI and hindIII. *The artificialRBS indicates the RBS of the F10 gene from T7 bacteriophage

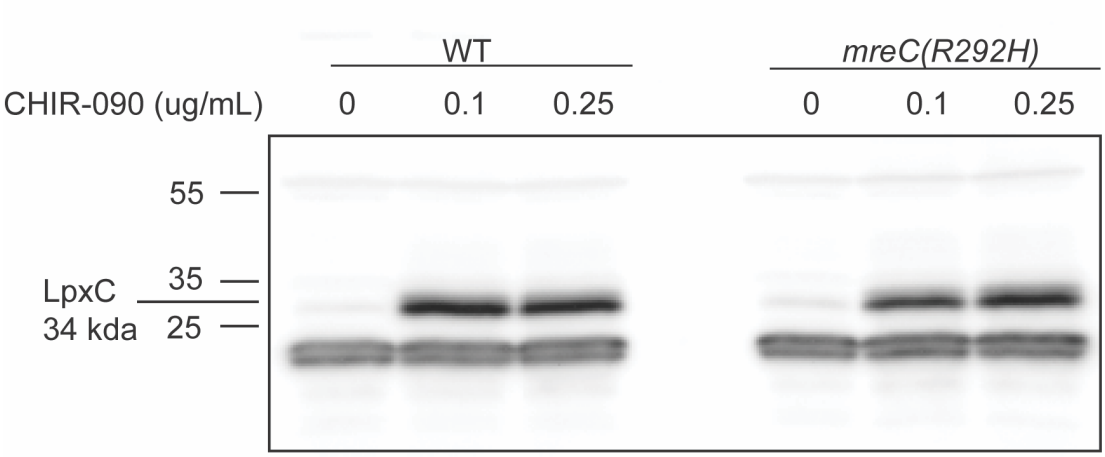

SI Figure 1: *mreC(R292H)* cells homeostatically regulate levels of LpxC in response to LpxC inhibitor CHIR-090. Immunoblot of LpxC levels in WT (HC555) and *mreC(R292H)* (PR5) cells treated with CHIR-090. Cells were grown for 24 hours at 30˚C in M9 + CAA + glu and then back diluted to OD_{600} = 0.05 in M9 + CAA + glu and incubated at 30˚C until OD_{600} = 0.4. Cells were gently pelleted and resuspended in LB and grown for one hour at 37˚C. CHIR-090 or DMSO was added to the cultures at the indicated concentrations. Cells were incubated for an additional hour at 37˚C before cell lysates were harvested for western blot.

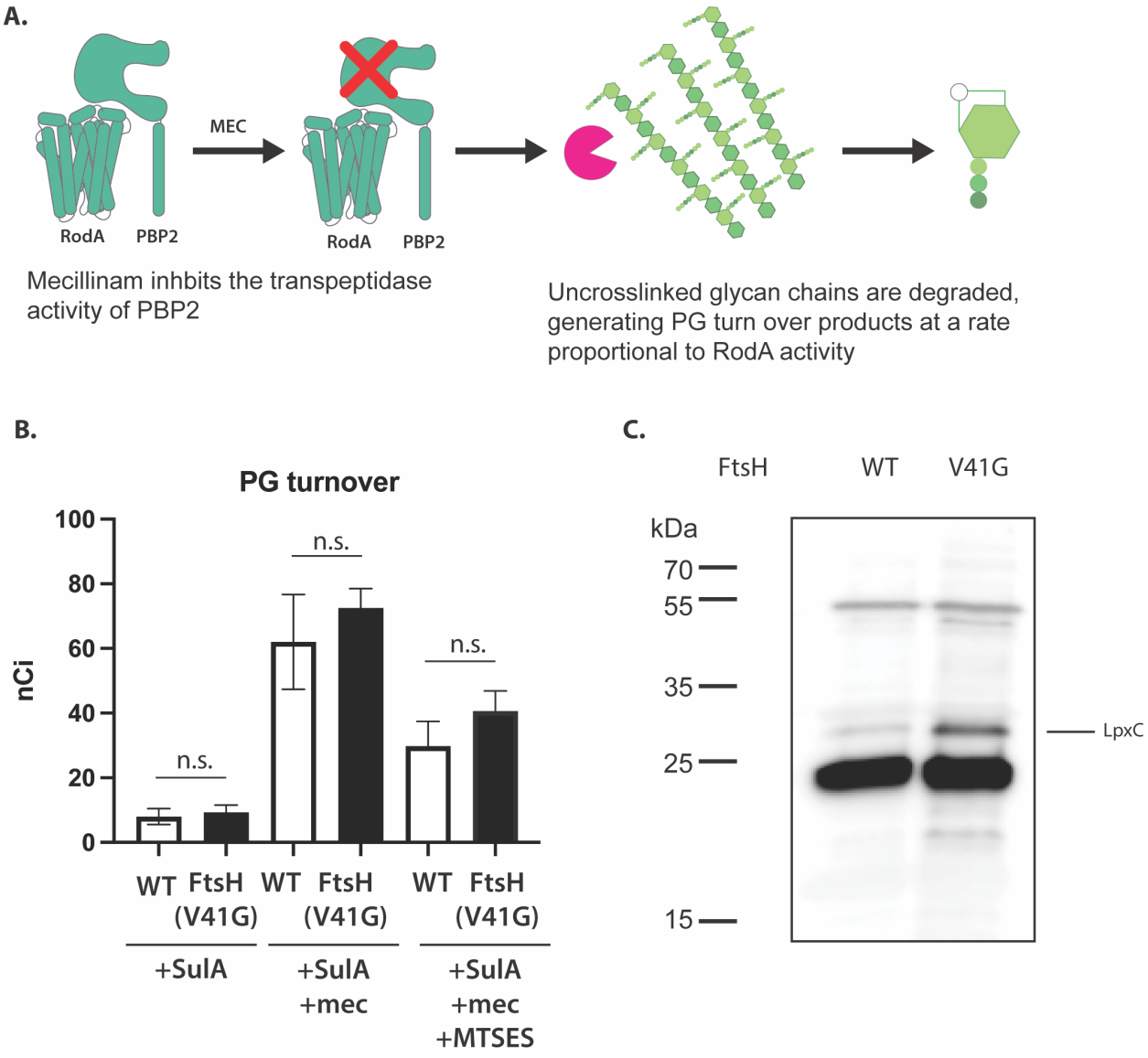

SI Fig. 2: *ftsH(V41G)* does not increase PG synthesis by the Rod complex. A. Schematic of the generation of peptidoglycan turnover products (adapted from Rohs et al. 2018(4)). Glycan chains are polymerized by the glycosyltransferase RodA and cross linked into the cell wall matrix by PBP2. Mecillinam blocks the transpeptidases activity of PBP2, leading to the accumulation of uncrosslinked glycan polymers, which are then degraded, generating PG turnover products. These products include a radiolabeled mDAP residue, allowing for detection via HPLC and in-line scintillation counting. **B.** The amount of PG turnover products in WT and FtsH(V41G) cells. SulA blocks divisome activity and MTSES blocks PG synthesis by class A PBPs. Statistical significance was determined using an Unpaired t-test (n.s. indicates not significant). **C.** Immunoblot of LpxC in strains used for radiolabeling assay (see materials and methods).

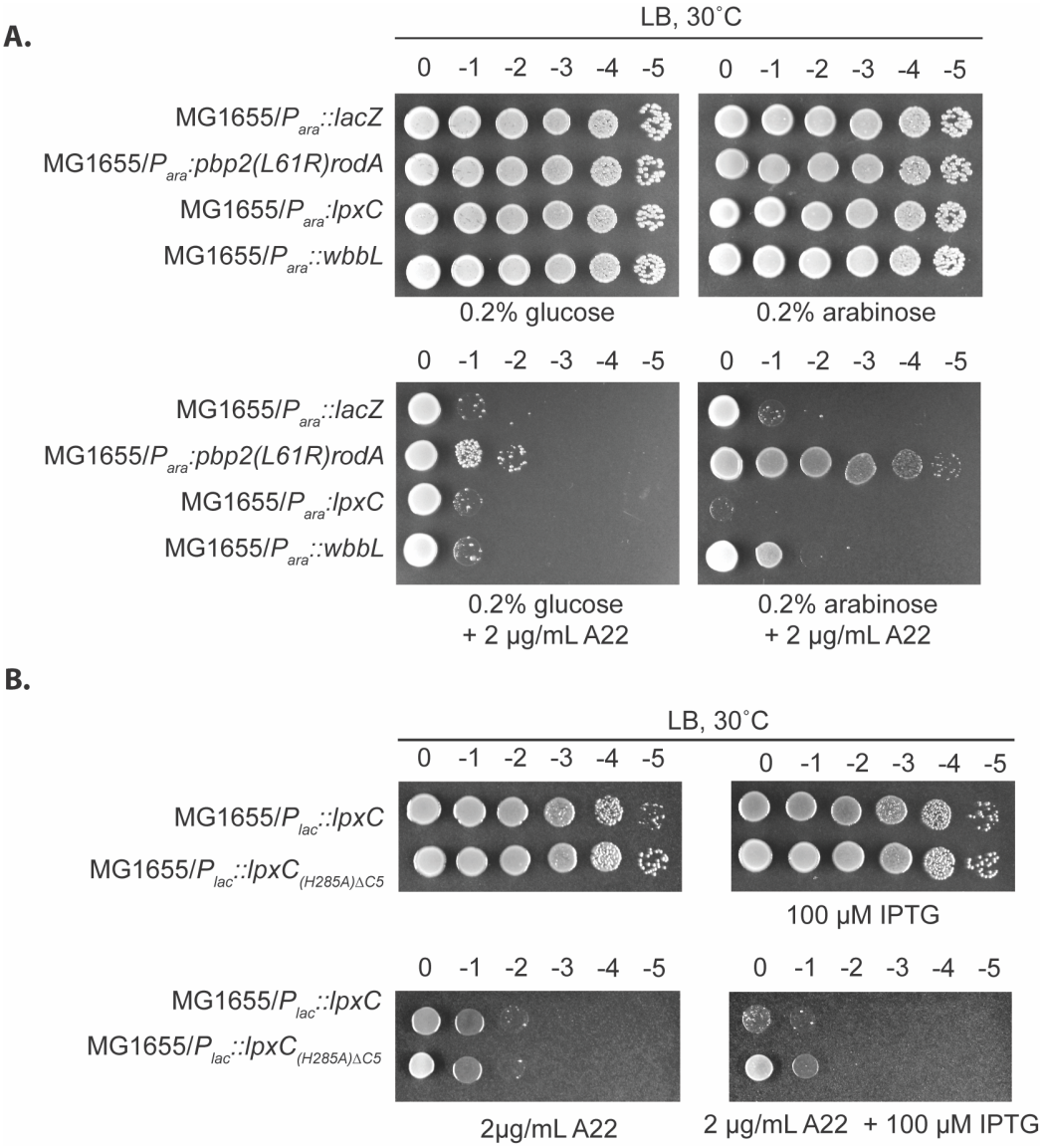

SI figure 3: Overexpressing *lpxC* or *wbbL* does not confer A22 resistance. A. MG1655 cells harboring arabinose-inducible plasmids expressing *lacZ* (pEMF134)*, pbp2(L61R)rodA* (pEMF131)*, lpxC* (pEMF112), or *wbbL* (pEMF130) were grown overnight in LB. Cultures were normalized to an OD_{600}=1, serially diluted, and spotted on LB + 0.2% glucose or 0.2% arabinose plates with and without 2 µg/mL A22. Plates were incubated at 30˚C for 24 hours. **B**. MG1655 cells harboring an IPTG-inducible plasmid expressing *lpxC* (pPR111) or *lpxC(H285A)ΔC5* (pPR115) were grown o/n at 30˚C in LB. Cultures were normalized to an OD_{600}=1, serially diluted, and spotted on LB plates with and without 100 µM IPTG and 2 µg/mL A22. Plates were incubated at 30˚C for 24 hours.

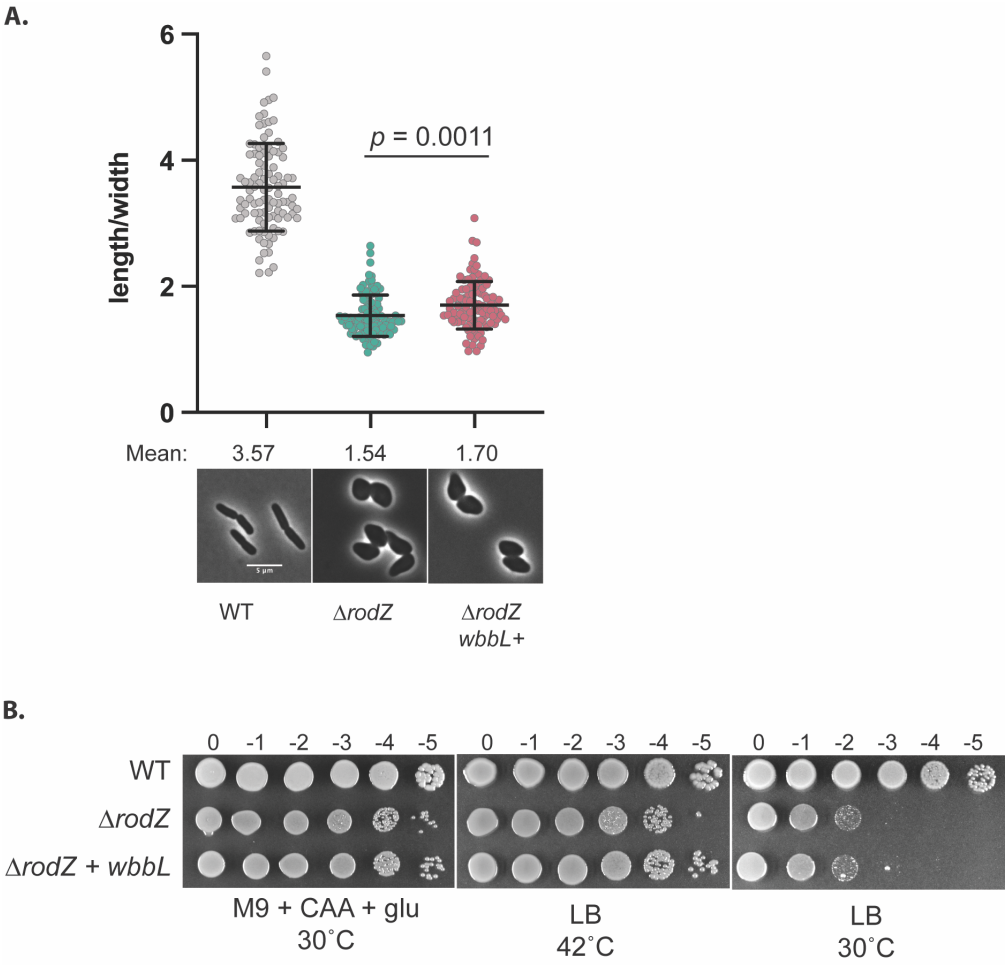

SI Figure 4: The overexpression of *wbbL* does not ameliorate the growth or shape defects of Δ*rodZ* cells. A. WT (EMF212), Δ*rodZ* (PR134), and Δ*rodZ wbbL*+ (EMF214) were cultures O/N in LB at 37˚C. Cultures were diluted at a ratio of 1:200 in LB and grown at 30˚C until OD_{600} = 0.3. Cells were then fixed and imaged. Aspect ratios were analyzed using the FIJI plugin MicrobeJ (5). Scale bar = 5 μm. n= 100 cells per group. Statistical significance determined using an Unpaired t test with Welch's correction (not assuming equal SDs). **B.** The strains listed in (A) were cultures in LB at 37˚C overnight. Cultures were normalized to OD_{600}=1, serially diluted, and spotted on M9 + CAA + glu or LB plates. LB plates were incubated for 16 hours and M9 + CAA + glu plates were incubated for 48h hours.

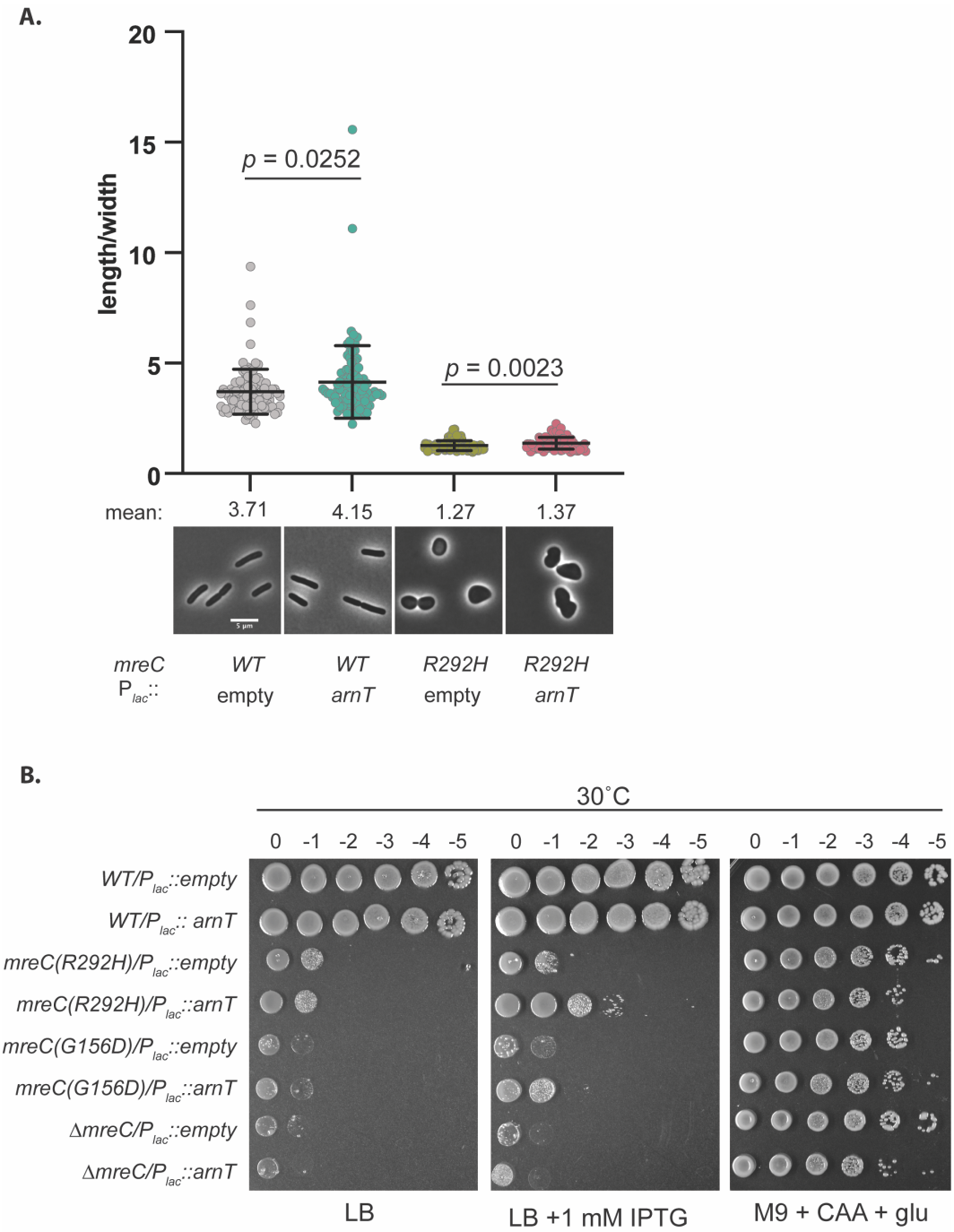

SI Figure 5: The overexpression of *arnT* partially ameliorates the growth defect of *mreC(R292H).* A. WT (HC555) or *mreC(R292H)* (PR5) harboring either the empty vector (pPR66) or an IPTG-inducible plasmid expressing *arnT* (pAF2) were grown for 24 hours at 30˚C in M9 + CAA + glu. Cells were diluted to OD_{600}= 0.05 in M9 + CAA + glu + 1mM IPTG and cultured at 30˚C until OD_{600}=0.2-03. Cells were then gently pelleted and resuspended in LB + 1mM IPTG and grown at 37˚C until OD_{600} = 0.3. Cells were then fixed and imaged. Aspect ratios were analyzed using the FIJI plugin MicrobeJ (5). Scale bar = 5 μm. n= 100 cells per group. Statistical significance determined using an Unpaired t test with Welch's correction (not assuming equal SDs). **B.** WT (HC555) or mreC(R292H) (PR5) harboring either the empty vector

(pPR66) or an IPTG-inducible plasmid expressing *arnT* (pAF2) were grown for 24 hours at 30˚C in M9 + CAA + glu. The overnight cultures were normalized to a OD_{600}=1, serially diluted, and spotted LB, LB + 1mM IPTG, and M9 + CAA + glu plates. LB plates were incubated at 30˚C for 24 hours and the M9 plates were incubated at 30˚C for 48 hours.

SI Movie 1: Time lapse of MreB in *wbbL(INS)* (AV007) and *wbbL (+)* (EMF210) cells expressing *mreC(R292H)D* (pMS9) described in Fig. 5. Three-minute timelapse series with an acquisition frame rate of 3s were recorded to capture MreB dynamics. TOP: ^{SW}*mreB-mNeon* overlayed over a single-frame phase contrast reference image. BOTTOM: Examples of MreB tracks identified using TrackMate (6, 7). Scale Bar = 2 μM.

Table S1: Suppressors of *mreC(R292H)* and *mreC(G156D)*

Suppressor	Background	Selection strategy	description
ftsH(V41G)	*mreC(G156D)*	Spontaneous suppressors, LB + 1% SDS at 30˚C	Inner membrane zinc-dependent metalloprotease that regulates the degradation of UDP-3-O-acyl-N-acetylglucosamine deacetylase (LpxC)(8, 9), the enzyme that catalyzes the first committed step in LPS synthesis (10, 11).
ftsH(F37V)	*mreC(R292H)*	Spontaneous suppressors, LB at 30˚C	
lapB(Δ379-389)	*mreC(G156D)*	Spontaneous suppressors, LB + 1% SDS at 30˚C	Lipopolysaccharide assembly protein B, mediates LpxC degradation by FtsH (12-14)

Table S2: Strains used in this study

Strain	Genotype[a]	Source/Reference[b]
AAY1	MG1655 *ΔlacIZYA<>frt wbbL+::kan*	(15)
AV007	MG1655 *mreB'-mNeon-'mreB ΔyhdE<> frt*	This study
Dh5a(lpir)	*F- hsdR17 deoR recA1 endA1 phoA supE44 thi-1 gyrA96 relA1 Δ(lacZYA-argF)U169 Ø80dlacZΔM15 λpir*	Laboratory strain
EMF150	MG1655 *ΔmreC::kan*	This study, MG1655 X P1(MT4/pTB63)
EMF196	MG1655 *leuU-cat-yhbX yrdE-kan*	This study, PR103 x P1(HC555)
EMF197	MG1655 *leuU-cat-yhbX yrdE-kan mreC(G156D)*	This study, PR103 x P1(PR30/pTB63)
EMF199	MG1655 *leuU-cat-yhbX ftsH(V41G) yrdE-kan*	This study, PR104 x P1(HC555)
EMF210	MG1655 *mreB'-mNeon-'mreB ΔyhdE<> frt wbbL+::kan*	This study, AV007 X P1(NR2528)(15)
EMF211	TB10 *wbbL(INS)::kan*	This study
EMF212	MG1655 *wbbL(INS)::kan*	This study, MG1655 x P1(EMF211)
EMF214	MG1655 *ΔrodZ::cat wbbL+::kan*	This study, PR134 X P1(NR2528)(15)
EMF52(attHKHC859)	MG1655 *ΔlysA<>FRT ΔpbpC<>FRT ΔmtgA<>FRT ΔampD<>FRT mrcB(S247C) mrcA<>FRT leuU-cat-yhbX ftsH(V41G)*	This study, HC533(attHKHC859) X P1(PR96)
EMF53(attHKpHC859)	MG1655 *ΔlysA<>FRT ΔpbpC<>FRT ΔmtgA<>FRT ΔampD<>FRT mrcB(S247C) mrcA<>FRT leuU-cat-yhbX*	This study, HC533(attHKHC859)(16) X P1(PR90)
EMF63	MG1655 *fabZ(sfhC21)*	This study, EMF61 X P1(AR3289)(8)

HC555	MG1655 *yrdE-kan*	(4)
JAB593	MG1655 *mreB'-mNeon-'mreB ΔyhdE::cat*	(4)
MG1655	rph1 lvG rfb-50	(17)
MT4/pTB63	MG1655 *ΔlacIZYA<>frt mreC::kan*	(4)
PR103	MG1655 *leuU-cat-yhbX*	This study,MG1655 x P1(PR90)
PR104	MG1655 *leuU-cat-yhbX ftsH(V41G)*	This study, MG1655 X P1(PR96)
PR109	MG1655 *leuU-cat-yhbX yrdE-kan mreC(R292H)*	This study, PR103 x P1(PR5/pTB63)
PR110	MG1655 *leuU-cat-yhbX ftsH(V41G) yrdE-kan mreC(R292H)*	This study, PR104 X P1(PR5/pTB63)
PR111	MG1655 *leuU-cat-yhbX ftsH(V41G)yrdE-Kan mreC(G156D)*	This study, PR104 X P1(PR30/pTB63)
PR134	MG1655 *ΔrodZ::cat*	(4)
PR30	MG1655 *mreC(G156D) yrdE-kan*	(4, 18)
PR39	MG1655 *mreC(R292H) pbp2(L61R) yrdE-kan*	(4)
PR5	MG1655 *mreC(R292H) yrdE-kan*	(4, 18)
PR82	MG1655 *mreC(R292H) yrdE-kan ftsH(F37V)*	This study
PR86	MG1655 *mreC(G156D) yrdE-kan lapB(Δ379-389)*	This study
PR88	MG1655 *mreC(G156D) yrdE-kan ftsH(V41G)*	This study
PR90	TB10 *leuU-cat-yhbX*	This study
PR96	MG1655 *leuU-cat-yhbX ftsH(V41G) yrdE-kan mreC(G156D)*	This study
TB10	MG1655 *λΔcro-bio nad::Tn10*	(19)
TB28	MG1655 *ΔlacIZYA::frt*	(20)

[a] The kanamycin resistance cassette (*kan*) and chlorophenicol resistance cassette (cat) are flanked by frt sequences for removal by FLP recombinase

[b] Strains generate by P1 transduction are described as follows: recipient strain X P1(donor strain) (See supplementary text for details)

Table S3: Plasmids used in this study

Plasmid	Relevant features[a]	Origin	Reference/source
pAF2	CM^R, P_{lac}::*artificalRBS_arnT*	pBR/colE1	This study
pcp20	CM^R, Amp^R, FLP+, lambda cI857+	pSC101	(3)
pEMF112	Tet^R, P_{ara}::*nativeRBS_lpxC*	pBR/colE1	This study
pEMF130	Tet^R , P_{ara}::*artificalRBS_wbbL*	pBR/colE1	This study
pEMF131	Tet^R, P_{ara}::*nativeRBS_ pbp2(L61R)rodA*	pBR/colE1	This study
pEMF134	Tet^R, P_{ara}::*artificalRBS_lacZ*	pBR/colE1	This study
pEMF137	CM^R, P_{lac}:: *nativeRBS_fabZ(L85P)*	pBR/colE1	This study
pEMF51	Tet^R, P_{ara}:: *nativeRBS_fabZ(L85P)*	pACYC	This study
pHC857	CM^R, P_{lac}::*nativeRBS_pbpA-rodA*	pBR/colE1	(16)
pHC859	Tet^R , P_{tac}::*sulA*	R6K	(16)
pKD46	Amp^R, P_{ara}::lambda red genes for recombineering	pSC101	(2)
pMS9	CM^R, P_{lac}:*nativeRBS_mreC(R292H)mreD*	pBR/colE1	(18)
pNP140	Tet^R, P_{ara}:: *sulA*	pACYC	This study
pNP146	Tet^R, P_{ara}::*sulA*	pBR/colE1	(21)
pPR111	CM^R, P_{lac}::*nativeRBS_lpxC*	pBR/colE1	(22)
pPR112	CM^R, P_{lac}::*nativeRBS_lpxCΔC5*	pBR/colE1	This study
pPR115	CM^R, P_{lac}::*nativeRBS (H285A)_lpxC*	pBR/colE1	This study
pPR122	CM^R, P_{lac}::*nativeRBS_pbpA(L61R)rodA*	pBR/colE1	This study

pPR66	CM^R, P_{lac}::empty	pBR/colE1	(22)
pTB63	Tet^R , P_{native}::*ftsQAZ*	pSC101	(23)

[a] P_{lac} and Pt_{ac} refer to the lactose promoters and P_{ara} refers to the arabinose promoter. The artificialRBS indicates the RBS of the Φ10 gene from T7 bacteriophage.

Table S4: Primers used in this study

Primer name	Sequence	Strain/plasmid
leuU-yhbX_P2_F	ACCTTGAAACGATGGTGCCGGTACGCCTTAG TTATAAATTCATATGAATATCCTCCTTAG	PR90
leuU-yhbX_P1_R	TTGACACAATAAAGTGCCAATTATGTCAGTAG AAGGGAAAGTGTAGGCTGGAGCTGCTTC	PR90
LpxC_nativeRBS_XbaI5	CCCCTCTAGATAATTTGGCGAGATAATACGAT GATC	pPR111
arnT_hindIII_R	TGATAAGCTTATCATTTGGGACGATACTGAAT CAGC	pAF2
arnT_xbal_F	CCCCTCTAGATTTAAGAAGGAGATATACATAT GAAATCGGTACGTTACCTTATCGG	pAF2
hindIII_fabZ_R	TACCAAGCTTTCAGGCCTCCCGGCTACG	pEMF51
hindIII_lacZ_R	TGATAAGCTTATTATTTTTGACACCAGACCAA CTGGTAATG	pEMF134
HindIII-pbpA	GCTAAAGCTTTTTATTCGGATTATCCGTCATG	pPR122
lpxC_3'truncation_HindIII	TGATAAGCTTATTAAGGCGCTTTGAAGGCCAA CGG	pPR112
lpxC_quickchange_H265A	TACCGCTTATAAATCCGGTGCTGCACTGAATA ACAAACTG	pPR115
lpxC_R_HindIII	TGATAAGCTTATTATGCCAGTACAGCTGAAGG CGC	pPR111
pEMF131_F	CAAATCTAGATAAGGGAGCTTTGAGTAG	pEMF131
pEMF131_R	TGATAAGCTTATGCGCACCTCTTACACGCTTT TC	pEMF131
wbbL XbaI-RBS-NdeI5'	TCTAGATTAAGAAGGAGATATACATATGGTAT ATATAATAATCGTTTCCCACGG	pEMF130
wbbL_HindIII_Rev	AAGCTTTTACGGGTGAAAAACTGATGAAATTC GATCAAAGTTGCG	pEMF130
wbbL_kan_F	TCGCAACTTTGATCGAATTTCATCAGTTTTTC ACCCGTAAGCGATTGTGTAGGCTGGAGC	EMF211
wbbL_kan_R	ATAAATAGCTTATCCATGCTTATATGCTTACG GCTTTATACTATTCCGAAGTTCCTATTC	EMF211

xbaI_fabZ_F	ATCCTCTAGATGTCGTTTCTTATATTTTGACA GGAAGAG	pEMF51
xbaI_strongRBS_lacZ	ATCCTCTAGACTTTAAGAAGGAGATATACCAT GACCATGATTACGGATTCACTGG	pEMF134
XbaI-pbpA	GCTATCTAGATAAGGGAGCTTTGAGTAGAAA ACG	pPR122

SI references

1. D. Yu *et al.*, An efficient recombination system for chromosome engineering in *Escherichia coli*. *Proc. Natl. Acad. Sci.* U.S.A. **97**, 5978-5983 (2000).
2. K. A. Datsenko, B. L. Wanner, One-step inactivation of chromosomal genes in *Escherichia coli* K-12 using PCR products. *Proc. Natl. Acad. Sci.* U.S.A. **97**, 6640-6645 (2000).
3. P. P. Cherepanov, W. Wackernagel, Gene disruption in *Escherichia coli*: TcR and KmR cassettes with the option of Flp-catalyzed excision of the antibiotic-resistance determinant. *Gene* **158**, 9-14 (1995).
4. P. D. Rohs *et al.*, A central role for PBP2 in the activation of peptidoglycan polymerization by the bacterial cell elongation machinery. *PLoS Genet.* **14**, e1007726 (2018).
5. A. Ducret, E. M. Quardokus, Y. V. Brun, MicrobeJ, a tool for high throughput bacterial cell detection and quantitative analysis. *Nat. Microbiol.* **1**, 1-7 (2016).
6. J.-Y. Tinevez *et al.*, TrackMate: An open and extensible platform for single-particle tracking. *Methods* **115**, 80-90 (2017).
7. D. Ershov *et al.*, TrackMate 7: integrating state-of-the-art segmentation algorithms into tracking pipelines. *Nat. Methods*, 1-4 (2022).
8. T. Ogura *et al.*, Balanced biosynthesis of major membrane components through regulated degradation of the committed enzyme of lipid A biosynthesis by the AAA protease FtsH (HflB) in *Escherichia coli*. *Mol. Microbiol.* **31**, 833-844 (1999).
9. K. Ito, Y. Akiyama, Cellular functions, mechanism of action, and regulation of FtsH protease. *Annu. Rev. Microbiol.* **59**, 211-231 (2005).
10. M. S. Anderson, A. D. Robertson, I. Macher, C. R. Raetz, Biosynthesis of lipid A in *Escherichia coli*: identification of UDP-3-O-[(R)-3-hydroxymyristoyl]-. alpha.-D-glucosamine as a precursor of UDP-N2, O3-bis [(R)-3-hydroxymyristoyl]-. alpha.-D-glucosamine. *Biochemistry* **27**, 1908-1917 (1988).
11. K. Young *et al.*, The envA permeability/cell division gene of *Escherichia coli* encodes the second enzyme of lipid A biosynthesis. UDP-3-O-(R-3-hydroxymyristoyl)-N-acetylglucosamine deacetylase. *J. Biol. Chem.* **270**, 30384-30391 (1995).
12. G. Klein, N. Kobylak, B. Lindner, A. Stupak, S. Raina, Assembly of lipopolysaccharide in Escherichia coli requires the essential LapB heat shock protein. *J. Biol. Chem.* **289**, 14829-14853 (2014).

13. S. Mahalakshmi, M. Sunayana, L. SaiSree, M. Reddy, yciM is an essential gene required for regulation of lipopolysaccharide synthesis in *Escherichia coli*. *Mol. Microbiol.* **91**, 145-157 (2014).
14. S. Shu, W. Mi, Regulatory mechanisms of lipopolysaccharide synthesis in *Escherichia coli. Nat. Commun.***13**, 1-11 (2022).
15. L. T. Sham, S. Zheng, A. A. Yakhnina, A. C. Kruse, T. G. Bernhardt, Loss of specificity variants of WzxC suggest that substrate recognition is coupled with transporter opening in MOP-family flippases. *Mol. Microbiol.* **109**, 633-641 (2018).
16. H. Cho, T. Uehara, T. G. Bernhardt, Beta-lactam antibiotics induce a lethal malfunctioning of the bacterial cell wall synthesis machinery. *Cell* **159**, 1300-1311 (2014).
17. M. Guyer, R. R. Reed, J. Steitz, K. Low (1981) Identification of a sex-factor-affinity site in E. coli as γδ. in *Cold Spring Harbor symposia on quantitative biology* (Cold Spring Harbor Laboratory Press), pp 135-140.
18. P. D. Rohs *et al.*, Identification of potential regulatory domains within the MreC and MreD components of the cell elongation machinery. *J. Bacteriol.* **203**, e00493-00420 (2021).
19. J. E. Johnson, L. L. Lackner, C. A. Hale, P. A. De Boer, ZipA is required for targeting of DMinC/DicB, but not DMinC/MinD, complexes to septal ring assemblies in *Escherichia coli. J. Bacteriol.* **186**, 2418-2429 (2004).
20. T. G. Bernhardt, P. A. De Boer, Screening for synthetic lethal mutants in *Escherichia coli* and identification of EnvC (YibP) as a periplasmic septal ring factor with murein hydrolase activity. *Mol. Microbiol.* **52**, 1255-1269 (2004).
21. J. A. Buss, N. T. Peters, J. Xiao, T. G. Bernhardt, ZapA and ZapB form an FtsZ-independent structure at midcell. *Mol. Microbiol.* **104**, 652-663 (2017).
22. E. M. Fivenson, T. G. Bernhardt, An Essential Membrane Protein Modulates the Proteolysis of LpxC to Control Lipopolysaccharide Synthesis in *Escherichia coli*. *mBio* **11**, e00939-00920 (2020).
23. F. O. Bendezú, P. A. De Boer, Conditional lethality, division defects, membrane involution, and endocytosis in mre and mrd shape mutants of *Escherichia coli*. *J. Bacteriol.* **190**, 1792-1811 (2008).